Exclusive diffractive processes and the quark substructure of mesons

M. A. Pichowsky
Physics Division, Argonne National Laboratory, Argonne, Illinois 60439-4843
and Department of Physics and Astronomy, University of Pittsburgh, Pittsburgh, Pennsylvania 15260

T.-S. H. Lee
Physics Division, Argonne National Laboratory, Argonne, Illinois 60439-4843
(Received 18 December 1996)

Exclusive diffractive processes on the nucleon are investigated within a model in which the quark-nucleon interaction is mediated by Pomeron exchange and the quark substructure of mesons is described within a framework based on the Dyson-Schwinger equations of QCD. The model quark-nucleon interaction has four parameters which are completely determined by high-energy πN and KN elastic scattering data. The model is then used to predict vector-meson electroproduction observables. The obtained ρ- and ϕ-meson electroproduction cross sections are in excellent agreement with experimental data. The predicted q^2 dependence of J/ψ-meson electroproduction also agrees with experimental data. It is shown that confined-quark dynamics plays a central role in determining the behavior of the diffractive, vector-meson electroproduction cross section. In particular, the onset of the asymptotic $1/q^4$ behavior of the cross section is determined by a momentum scale that is set by the current-quark masses of the quark and antiquark inside the vector meson. This is the origin of the striking differences between the q^2 dependence of ρ-, ϕ-, and J/ψ-meson electroproduction cross sections observed in recent experiments. [S0556-2821(97)01415-X]

PACS number(s): 13.60.Le, 12.38.Aw, 13.60.Fz, 24.85.+p

I. INTRODUCTION

At high energies, the differential cross sections for hadron-hadron elastic scattering are forward peaked and fall off exponentially in the small-momentum-transfer region. The magnitudes of these cross sections increase very slowly with energy at a rate that seems to be independent of the hadrons involved. The mechanism responsible for this behavior was originally identified as *Pomeron exchange* within Regge phenomenology [1,2]. Since the advent of quantum chromodynamics (QCD) as the underlying theory of strong interactions, there has been considerable effort towards the development of a description of Pomeron exchange directly in terms of QCD. However, a satisfactory description has not yet been obtained. The objective of this work is to develop an understanding of the role played by the quark substructure of hadrons in diffractive processes as a step towards providing a description of Pomeron exchange in terms of the quark and gluon degrees of freedom of QCD. In particular, we explore the consequences of nonperturbative-quark dynamics, such as confinement and dynamical chiral symmetry breaking, in determining observables that are accessible in current experiments at the Deutsches Elektronen-Synchrotron (DESY), Thomas Jefferson National Accelerator Facility (TJNAF), and Fermi National Accelerator Laboratory (Fermilab). The availability of high-quality data from these facilities provides a means to explore the dynamical content of Pomeron exchange which, in turn, has motivated recent theoretical effort in this direction.

It is generally believed that the underlying mechanism responsible for Pomeron exchange is multiple-gluon exchange. This idea was first investigated by Low within the Bag model [3] and by Nussinov in Ref. [4]. The simplest multiple-gluon exchange requires at least two gluons, since all hadrons are color singlets. As there are many different ways in which two gluons can be exchanged between two hadrons, a straightforward calculation of two-gluon exchange is difficult. For example, in pion-nucleon elastic scattering, there are several ways in which the quarks inside the two hadrons can propagate and exchange gluons. One contribution arises when the quark inside the pion exchanges two gluons with a quark inside the nucleon. Another possibility is that the two exchanged gluons interact with two different quarks inside the nucleon. There are other possibilities as well. To further complicate matters, the exchanged gluons can interact with each other. Such a calculation cannot at present be carried out without making additional approximations.

A simplification was introduced by Donnachie and Landshoff [5], who proposed that the Pomeron couples to the nucleon like an isoscalar photon. This led them to consider a model in which multiple-gluon exchange is replaced by a Regge-like Pomeron exchange whose coupling to the nucleon is described in terms of a nucleon isoscalar electromagnetic (EM) form factor. In our work, we employ a similar approach, thereby avoiding the complexities associated with the quark substructure of the nucleon so that we may focus on exploring the dynamics of Pomeron exchange and its relation to the quark substructure of mesons. The model of Ref. [5] has also been applied to ρ-meson electroproduction [6] with the simplifying assumption that the quark propagators inside the ρ meson can be factorized out of the quark-loop integration, replaced by constituent-quark propagators and evaluated at a single momentum. A ramification of employing such a procedure is the loss of some of the momentum dependence originating from the quark substructure of the vector meson. Consequently, agreement with experimental data requires the introduction of a quark-Pomeron

form factor which is, in fact, dependent on the type of vector meson produced (e.g., ρ, ϕ, J/ψ) [7]. However, when the quark substructure of the vector meson is properly accounted for, *no* quark-Pomeron form factor is required to obtain agreement with ρ-meson electroproduction data [8]. The extent to which the same is true for other vector mesons is addressed in this work.

The first objective of this investigation is to construct a model which restores some of the important features of QCD and nonperturbative-quark propagation to the study of Pomeron exchange and the role of the quark substructure of mesons in diffractive processes. Some nonperturbative aspects of QCD, such as quark and gluon confinement, are expected to play important roles in exclusive processes [9]. We find that incorporating such features into the model considered herein, naturally leads to predictions in agreement with the observed q^2 dependence of ρ-, ϕ-, and J/ψ-meson electroproduction cross sections, within a single framework and *without* introducing quark-Pomeron form factors.

The second objective of this investigation is to use the constructed model to determine the extent to which Pomeron exchange can be interpreted within QCD as multiple-gluon exchange. There have been some experimental observations that support this notion and numerous theoretical investigations on the subject, starting with those in Refs. [3,4]. One such experimental observation is the near flavor *independence* of high-energy meson-nucleon elastic scattering amplitudes. If Pomeron exchange is predominantly gluons, then flavor dependence observed in the diffractive processes of light quarks, should arise mostly from the quark substructure of the hadrons involved. A satisfactory resolution of this outstanding problem requires that cross sections for diffractive processes are calculated from a model in which the perturbative and nonperturbative properties of quarks, confined within hadrons, are accounted for. That is, the model employed should have the properties expected from nonperturbative QCD and provide a good description of the low-energy properties of hadrons, such as their EM form factors and magnetic moments. Therefore, in this work, we use the confined-quark propagator and Bethe-Salpeter (BS) amplitudes obtained from phenomenological studies of hadrons based on the Dyson-Schwinger equations (DSE's) of QCD.

The DSE's are an infinite set of coupled integral equations that relate all of the n-point functions of a quantum field theory to each other. The generating functional of a quantum field theory being completely determined once all of the n-point functions are known. Hence, knowledge of the n-point functions completely specifies the dynamics of the theory. The simplest of these is the two-point, quark-propagator DSE, which describes how dressing of the quark propagator is dynamically generated by the quark's interactions with its own gluon field. To obtain a solution of this integral equation requires knowledge of other n-point functions, which in turn, satisfy their own DSE's. In general, the kernel of a DSE that determines an n-point function contains at least one m-point function with $m>n$. This illustrates the self-coupling between the equations that necessarily entails a truncation scheme in order to obtain a finite and tractable set of equations. Quantitative studies of such truncated systems of DSE's have had considerable success; a review of this body of work may be found in Ref. [10].

The quark propagator employed herein is based on that obtained in a numerical study of the DSE's using a model-gluon propagator [11]. The obtained quark propagator exhibits its dynamical chiral symmetry breaking and confinement, both of which are essential to provide a good description of nonperturbative QCD phenomena. The significance of their role in diffractive processes is discussed later. Here, we only mention that the confined-quark propagator and BS amplitudes obtained from phenomenological studies of the DSE's provide an excellent description of processes involving mesons. Some of these processes include the π- and K-meson EM form factors [12], $\pi\pi$ scattering [13], $\rho\omega$ mixing [14], the $\gamma\pi^*\rightarrow\pi\pi$ form factor [15], the $\gamma^*\pi\gamma$ transition form factor [16], and various EM and weak decays of the π and K mesons [12,13,17]. The use of a confined-quark propagator distinguishes our approach from previous studies of Pomeron exchange and we find that it is essential in obtaining a consistent description of vector-meson electroproduction for both large and small values of the photon momentum squared q^2.

With the confined-quark propagator and Bethe-Salpeter amplitudes taken from phenomenological DSE studies, the parameters of the quark-nucleon Pomeron-exchange interaction, introduced herein, are *completely determined* by πN and KN elastic scattering data. The model interaction is then used to investigate vector-meson electroproduction, which is currently the focus of great experimental and theoretical interest. We first consider exclusive ρ-meson electroproduction and then ϕ- and J/ψ-meson electroproduction.

The q^2 dependence of the vector-meson electroproduction cross sections obtained is particularly interesting. For large q^2, these cross sections obey an asymptotic power law, proportional to $1/q^4$. The transition to this asymptotic behavior is determined by the current-quark masses of the quark and antiquark inside the vector meson. It follows that the electroproduction cross sections of vector mesons comprised of heavy quarks exhibit this transition at a higher q^2 than those comprised of light quarks. This feature is demonstrated by an application of our model to ρ-, ϕ-, and J/ψ-meson electroproduction. Our predictions for the q^2 dependence of ρ-, ϕ-, and J/ψ-meson electroproduction cross sections are in excellent agreement with the recent experimental data.

At present several theoretical investigations of diffractive vector-meson electroproduction appear in the literature. Some of these employ perturbative methods [18–24] while others (including the present study) employ nonperturbative methods [5–7,25,26]. The range of applicability of perturbation theory in determining diffractive vector-meson electroproduction amplitudes at energies reached at the DESY ep collider HERA is still under discussion. In Ref. [18], it is argued that only the electroproduction of *longitudinally* polarized vector mesons should be considered and even then only at large photon momentum squared q^2. It has also been suggested that perturbative methods would only be reliable for the production of heavy-quark vector mesons [20]. This is supported by the experimental data for J/ψ-meson electroproduction which appear to be well described using such methods [19], while nonperturbative effects, such as the relative, ''Fermi momentum'' between the quark and antiquark

inside the vector meson, must be included when considering light-quark vector meson electroproduction [23].

Although there are similarities between these perturbative approaches and the approach considered herein, there is an important difference. For large photon momentum squared, the perturbative description of diffractive electroproduction proceeds by a mechanism in which the photon fluctuates into a quark-antiquark pair that then scatters elastically from the proton target and ultimately forms the on-mass-shell vector meson. It is assumed that the quark and antiquark each carry a large fraction of the total photon momentum and can therefore be treated as freely propagating, on-mass-shell partons in order to determine the $\overline{q}q$-proton elastic scattering amplitude. In contrast to this, we find that the presence of the vector meson bound state amplitude constrains the momentum flow in the quark loop so that one of the quark propagators that couples to the quark-photon vertex is hard and the other is soft. (This feature was first observed in Ref. [6] and is shown in Sec. IV to be true in our model as well.) An important ramification of this is that the asymptotic limit of the quark-photon vertex γ_μ does not provide the dominant contribution to the electroproduction cross section for any value of q^2. The Ward-Takahashi identity requires that *both* fermion legs must carry large momentum before the perturbative limit is reached; the presence of a vector-meson Bethe-Salpeter amplitude keeps this from happening in diffractive vector-meson electroproduction.

As an example of the importance of the nonperturbative contributions to the quark-photon vertex, we make predictions for the ratio of the longitudinal to transverse vector-meson electroproduction cross sections, $R=\sigma_L/\sigma_T$. We obtain a value of R that is much smaller than other models and smaller than the values extracted from ρ-meson electroproduction polarization data under the assumption of s-channel helicity conservation. Replacing the dressed quark-photon vertex by a bare vertex γ_μ reduces the value of R which gives an indication of the sensitivity of this observable to nonperturbative contributions in our model.

The organization of this paper is as follows. In Sec. II, we give a precise formulation of the quark-nucleon Pomeron-exchange interaction to be considered in this work. The parameters of the model are determined in Sec. III by considering πN and KN elastic scattering data. The model is applied to vector meson electroproduction and the results are presented in Sec. IV. Finally, in Sec. V, we present our conclusions.

II. A POMERON-EXCHANGE MODEL OF THE QUARK-NUCLEON INTERACTION

We begin by constructing a phenomenological model of the interaction between a quark, confined within a hadron, and an on-mass-shell nucleon. We only consider processes in which *no* flavor is exchanged between the quark and nucleon, so that in the high-energy and small-momentum-transfer region, this interaction can be parametrized in terms of *Pomeron exchange*. The most general form of the quark-nucleon Pomeron-exchange interaction may be represented as the shaded box in Fig. 1 and written in momentum space as

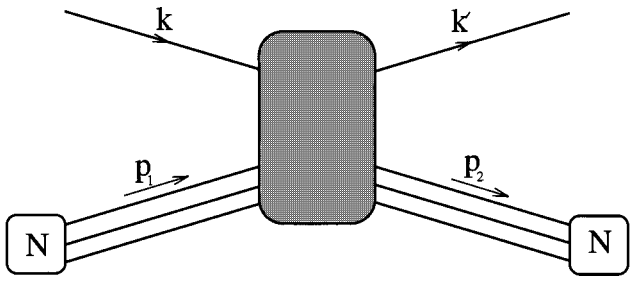

FIG. 1. General interaction between an on-mass-shell nucleon and confined quark, given by Eq. (2.6).

$$\mathcal{I}(k,k';p_1,p_2)=\sum_{\mu\nu f}\overline{q^f}(k')\Gamma^f_\mu q^f(k)\mathbf{G}_{\mu\nu}(k,k';p_1,p_2)\times\overline{u_{m'}}(p_2)\Gamma_\nu u_m(p_1), \tag{2.1}$$

where $u_m(p_1)$ and $\overline{u_{m'}}(p_2)$ are the Dirac spinors for the incoming and outgoing nucleons, $q^f(k)$ and $\overline{q^f}(k')$ are elements of the Grassmann algebra for a quark of flavor $f=u,d,s,\ldots$, Γ_ν is a matrix in the Dirac space of the nucleon, and Γ^f_μ is a matrix in the Dirac and flavor spaces of the quark. The momentum dependence of the exchange mechanism and the quark-Pomeron and nucleon-Pomeron couplings is given by the amplitude $\mathbf{G}_{\mu\nu}(k,k';p_1,p_2)$. In Eq. (2.1) and throughout this work, we have suppressed color and Dirac indices. We employ the Euclidean metric $\delta_{\mu\nu}=\mathrm{diag}(1,1,1,1)$ and Hermitian Dirac matrices that satisfy $\{\gamma_\mu,\gamma_\nu\}=2\delta_{\mu\nu}$.

The Pomeron-exchange model of the quark-nucleon interaction, employed throughout this work, is constructed from Eq. (2.1) by introducing the following three simplifying assumptions.

(i) Motivated by the observation that the differential cross sections of πN and KN elastic scattering have similar t dependence, we assume that the quark-Pomeron coupling Γ^f_μ can be factorized into two independent matrices:

$$\Gamma^f_\mu\to\Gamma_\mu\beta_f, \tag{2.2}$$

where Γ_μ is a constant matrix in the Dirac space of the quarks and β_f is a constant. This leads to the simplification that apart from a flavor-dependent overall multiplicative constant β_f, the quark-Pomeron coupling is flavor *independent*.

The use of a flavor-dependent coupling constant β_f is *not* inconsistent with the identification of Pomeron exchange as a multiple-gluon exchange. In contrast to the bare quark-gluon vertex (which is flavor independent) the nonperturbative dressing of the quark-gluon vertex *required* by the Slavnov-Taylor identity, introduces a nontrivial flavor dependence in Γ^f_μ.

Therefore, Eq. (2.2) incorporates the assumption that all of the flavor dependence of the quark-Pomeron-exchange vertex can be absorbed into a *constant* β_f. We will see that this minimal flavor dependence is sufficient to describe processes involving light quarks. However, in Sec. IV C, we show it is too restrictive to describe processes involving heavy quarks, such as J/ψ-meson electroproduction, and must be relaxed in this case.

(ii) We assume that the Dirac structure of the quark-Pomeron-exchange coupling in Eq. (2.2) and the nucleon-Pomeron-exchange coupling in Eq. (2.1) can be taken as $\Gamma_\mu = \gamma_\mu$. Although this assumption is overly simplistic and perhaps, dubious, it has been employed in previous works [5–8] and by maintaining this assumption, we can directly compare our results to these studies. Furthermore, the above assumption leads to approximate s-channel helicity conservation which is often associated with Pomeron exchange.

The dubious aspect of employing γ_μ as the quark-Pomeron-exchange vertex lies in the fact that γ_μ is odd under charge conjugation, while Pomeron-exchange should be even. In this work, the charge-conjugation parity of the quark-Pomeron-exchange coupling is implemented by hand. In our approach, we can investigate the possibility of a more sophisticated quark-Pomeron-exchange vertex, which has the supposed symmetries of Pomeron exchange. Such a study is left to future work.

(iii) The quark-nucleon Pomeron-exchange interaction $\mathbf{G}_{\mu\nu}(k,k';p_1,p_2)$ is assumed to be independent of the square of the four momenta of the quarks k^2 and k'^2 and diagonal in the Lorentz indices. Hence, we write $\mathbf{G}_{\mu\nu}(k,k';p_1,p_2)=\delta_{\mu\nu}\widetilde{G}(s,t)$, where $s=-(k+p_1)^2$ and $t=-(p_1-p_2)^2$. To make contact with previous Pomeron-exchange models [5,6], we introduce the parametrization

$$\widetilde{G}(s,t)\equiv 3\beta_u G(s,t)F_1(t), \tag{2.3}$$

where

$$F_1(t)\equiv \frac{4M_N^2-2.8t}{4M_N^2-t}\,\frac{1}{(1-t/t_0)^2} \tag{2.4}$$

is the nucleon isoscalar EM form factor, M_N is the nucleon mass, and $t_0 = 0.7\ \mathrm{GeV}^2$. The appearance of the EM form factor $F_1(t)$ in Eq. (2.3), suggests a similarity between photon and Pomeron exchange. The difference between these two exchanges is provided by the function $G(s,t)$ which is parametrized as

$$G(s,t)=(\alpha_1 s)^{\alpha_0+\alpha_1 t} \tag{2.5}$$

and is reminiscent of the Pomeron-exchange Regge trajectory discussed in Refs. [1,2]. Of course, by employing a value of $\alpha_0>0$, we recover the observed behavior that cross sections of processes which proceed through Pomeron exchange increase with energy $\sqrt{s}$.

With the above assumptions, Eq. (2.1) is reduced to

$$I(k,k';p_1,p_2)=\left[\sum_f \overline{q^f}(k')\beta_f\gamma_\mu q^f(k)\right][3\beta_u G(s,t)F_1(t)]$$
$$\times[\overline{u}_{m'}(p_2)\gamma_\mu u_m(p_1)]. \tag{2.6}$$

Although our model interaction, defined by Eq. (2.6), is similar in appearance to that of other authors [5,7], our description of the quark substructure of mesons differs significantly and plays a pivotal role in the processes considered.

Another difference between our approach and those of previous authors is our assumption that the quark coupling to the Pomeron-exchange interaction is independent of the quark four momenta k^2 and k'^2. Other authors have found it necessary to weaken this assumption by introducing an additional dependence on the quark momenta in the form of a ''quark-Pomeron form factor'' [6,7]. The scale associated with this form factor turns out to be flavor *dependent* [7], thereby violating our first assumption, as well. In our approach, we do not introduce this additional momentum dependence. In fact, we show that the flavor dependence of our predictions is entirely determined by the overall, multiplicative constant β_f and the quark substructure of the mesons involved. Having parametrized the quark-nucleon Pomeron-exchange interaction in Eqs. (2.5) and (2.6), we now proceed to determine the parameters.

Throughout this work we assume $\mathrm{SU}(2)_{\mathrm{flavor}}$ is a good symmetry, so that $\beta_d=\beta_u$. Hence, the four parameters α_0, α_1, β_u, and β_s completely determine the quark-nucleon Pomeron-exchange interaction for the light, u, d, and s quarks according to Eqs. (2.5) and (2.6). In Sec. III, these parameters are determined by considering πN and KN elastic scattering.

III. ELASTIC SCATTERING OF PSEUDOSCALAR MESONS AND NUCLEONS

The first application of our model is to obtain cross sections for πN and KN elastic scattering. This requires a description of the π- and K-meson quark-antiquark bound states. Such a description is provided for by phenomenological studies of the DSE's of QCD.

In Ref. [12], confined u-, d-, and s-quark propagators and π- and K-meson Bethe-Salpeter amplitudes were obtained and shown to provide an excellent description of π- and K-meson observables, including their EM form factors. These elements, having been previously determined in Ref. [12], allow us to use the existing πN and KN elastic scattering data to completely determine the parameters α_0, α_1, and β_f $(f=u,d,s)$ in the quark-nucleon Pomeron-exchange interaction of Eqs. (2.5) and (2.6).

Of the parameters α_0,α_1, and β_f $(f=u,d,s)$, α_0 is an observable, directly related to the universal s dependence of hadron-hadron total cross sections. Its value can, therefore, be taken from the analysis of experimental data given in Ref. [27]. In this study, it was found that the data for pp and $\overline{pp}$ total cross sections are best reproduced by the value of $\alpha_0=0.096^{+0.012}_{-0.009}$. For our purposes, $\alpha_0=0.10$ is sufficient. Our task is then to determine α_1 and β_f from πN and KN elastic scattering data.

Assuming $\mathrm{SU}(2)_{\mathrm{flavor}}$ symmetry for the u and d quarks, we set $\beta_d=\beta_u$. The parameters β_u and α_1 are determined by considering the πN elastic scattering differential cross section and β_s is determined by the *magnitude* of the KN elastic scattering cross section. The t dependence of the KN differential cross section is the first prediction of our model. In our approach, the t dependence of the quark-nucleon Pomeron-exchange interaction $G(s,t)$ in Eq. (2.5) is the *same* for all processes involving light quarks. Therefore, the predicted differences in the differential cross sections for πN and KN elastic scattering are *entirely* due to the quark substructure of the π and K mesons. To our knowledge, this is the first work to correlate the πN and KN differential cross sections and (as we will see) properly account for the

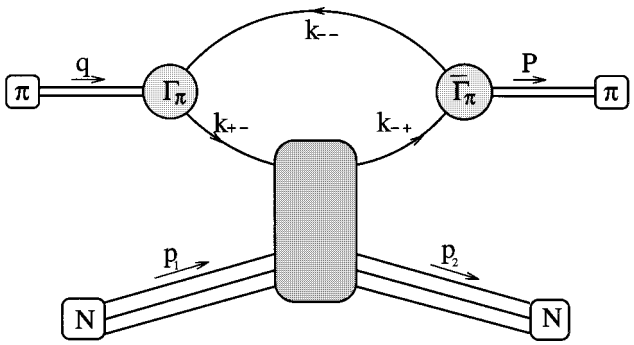

FIG. 2. One of two diagrams that contributes to πN elastic scattering in impulse approximation.

observed differences between them.

Pion-nucleon elastic scattering. The πN elastic scattering amplitude is described within our model as Pomeron exchange between the nucleon and the quark or antiquark inside the π meson. This is illustrated in Fig. 2. Application of the quark-nucleon Pomeron-exchange interaction defined by Eq. (2.6) leads to the πN scattering amplitude

$$\langle P;p_2m'|T_{\pi N\to\pi N}|q;p_1m\rangle = 2i\Lambda_\mu(q,P)\ \ [3\beta_u F_1(t)G(s,t)][\,\overline{u}_{m'}(p_2)\gamma_\mu u_m(p_1)]. \tag{3.1}$$

Here, $\Lambda_\mu(q,P)$ describes the coupling of a π meson to the Pomeron-exchange interaction and the remaining terms were defined in Sec. II. In deriving the product form of Eq. (3.1), we have assumed that the s dependence of the Pomeron-exchange interaction $G(s,t)$ can be evaluated from the external pion and nucleon momenta, so that $s=-(q+p_1)^2$ is the usual Mandelstam variable. This approximation is commonly employed in Pomeron-exchange models [5–7]. It is adopted here to ensure that the $\Lambda_\mu(q,P)$ is a function of q and P only, which reduces the number of integrations required to evaluate $\Lambda_\mu(q,P)$. We have found that this approximation can, at most, lead to a 10% change to the normalization of the amplitude and has no observable effect on the s and t dependence.

For π^+N elastic scattering, $\Lambda_\mu(q,P)$ is comprised of two terms:

$$\Lambda_\mu(q,P)=\Lambda^u_\mu(q,P)+\Lambda^{\bar d}_\mu(q,P), \tag{3.2}$$

where

$$\Lambda^u_\mu(q,P)=N_c\ \mathrm{tr}\int\frac{d^4k}{(2\pi)^4}S_u(k_{+-})\Gamma_\pi(k-\tfrac{1}{2}P) \times S_d(k_{--})\overline{\Gamma}_\pi(k-\tfrac{1}{2}q)S_u(k_{-+})\beta_u\gamma_\mu, \tag{3.3}$$

$$\Lambda^{\bar d}_\mu(q,P)=N_c\ \mathrm{tr}\int\frac{d^4k}{(2\pi)^4}S_d(k_{+-})\overline{\Gamma}_\pi(k-\tfrac{1}{2}P) \times S_u(k_{--})\Gamma_\pi(k-\tfrac{1}{2}q)S_d(k_{-+})\beta_d\gamma_\mu. \tag{3.4}$$

Here, $S_f(k)$ is the propagator for a quark of flavor f, $\Gamma_\pi(k)$ is the pion Bethe-Salpeter amplitude, $k_{\alpha\beta}=(k+(\alpha/2)q+(\beta/2)P)$, $N_c=3$ is the number of colors, and the trace is over Dirac indices. The kinematical variables for evaluating Eqs. (3.3) and (3.4) are also indicated in Fig. 2. The small mass difference between the u and d quarks is ignored and hence we take $S_u(k)=S_d(k)$. In this case, $\Lambda^u_\mu(q,P)$ and $\Lambda^{\bar d}_\mu(q,P)$ contribute equally to π^+N elastic scattering.

TABLE I. Confined-quark propagator parameters for u, d, and s quarks from Ref. [53]. An entry of ''same'' for s quark indicates that the value of the parameter is the same as u and d quarks.

f	b_0^f	b_1^f	b_2^f	b_3^f	$C^f_{m_f=0}$	$C^f_{m_f\neq0}$	m_f
u,d	0.131	2.90	0.603	0.185	0.121	0.00	5.1 MeV
s	0.105	same	0.740	same	1.69	same	127.5 MeV

In a general covariant gauge, the propagator for a quark of flavor f is

$$S_f(k)=-i\gamma\cdot k\sigma_V^f(k^2)+\sigma_S^f(k^2), \tag{3.5}$$

and its inverse is

$$S_f^{-1}(k)=i\gamma\cdot kA_f(k^2)+B_f(k^2). \tag{3.6}$$

Studies of the two-point quark DSE, employing a model-gluon propagator, suggest that the qualitative features of the confined-quark propagator are well described by the algebraic form [11]

$$\overline{\sigma_S^f}(x)=\frac{1-e^{-b_1^fx}}{b_1^fx}\frac{1-e^{-b_3^fx}}{b_3^fx}\left(b_0^f+b_2^f\frac{1-e^{-\Lambda x}}{\Lambda x}\right) +\overline{m}_f\frac{1-e^{-2(x+\overline{m}_f^2)}}{x+\overline{m}_f^2}+C^f_{m_f}e^{-2x},$$

$$\overline{\sigma_V^f}(x)=\frac{2(x+\overline{m}_f^2)-1+e^{-2(x+\overline{m}_f^2)}}{2(x+\overline{m}_f^2)^2}, \tag{3.7}$$

where $x=k^2/\lambda^2$, $\overline{\sigma_S^f}=\lambda\sigma_S^f$, $\overline{\sigma_V^f}=\lambda^2\sigma_V^f$, $m_f=\lambda\overline{m}_f$ is the bare mass for a quark of flavor f, $\Lambda=10^{-4}$, and $\lambda=0.566$ GeV is a momentum scale. All of the parameters and variables appearing in Eqs. (3.7) are dimensionless as they have been rescaled by λ. The value $\Lambda=10^{-4}$ is introduced only to ensure the decoupling of the small and intermediate k^2 behavior in the algebraic form, characterized by the parameters b_0^f and b_2^f, which is observed in numerical studies of the quark DSE.

The parameters b_0^f, b_1^f, b_2^f, b_3^f, $C^f_{m_f}$, and m_f for $f=u,d,s$ are determined in Ref. [12] by performing a χ^2 fit to experimental values of decay constants f_π, f_K, $\pi\pi$ scattering lengths, π- and K-meson electromagnetic form factors, charge radii, and other π- and K-meson observables. The resulting values of the parameters are given in Table I.

The algebraic forms for $\sigma_S^f(k^2)$ and $\sigma_V^f(k^2)$ are *analytic* everywhere in the finite complex k^2 plane. This ensures that the quark propagator $S_f(k)$ has no Lehmann representation and hence there are no quark-production thresholds in the

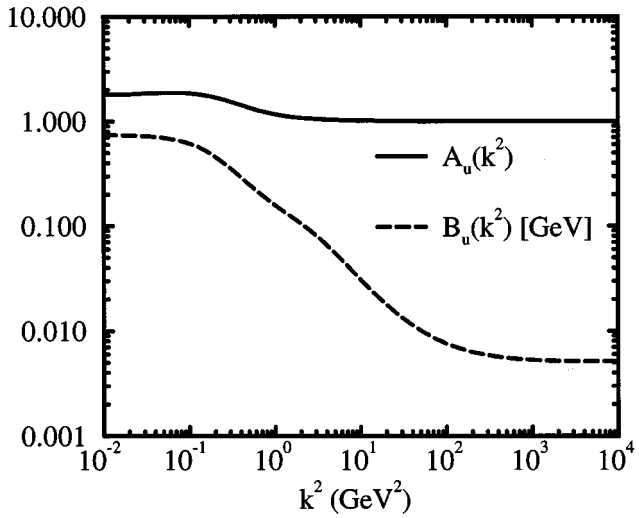

FIG. 3. The Lorentz-invariant functions $A_u(k^2)$ and $B_u(k^2)$ for the confined, u-quark propagator defined in Eqs. (3.7).

calculation of observables. The absence of such thresholds admits the interpretation that $S_f(k)$ describes the propagation of a *confined* quark.

It is possible that the *exact* quark propagator, obtained directly from the quark DSE of QCD, may have singularities or branch cuts (perhaps both) somewhere in the complex-k^2 plane. In this case, the forms given in Eqs. (3.7) are to be considered as approximate and only applicable within some region of Euclidean space. In the present study, the quark propagator in Eqs. (3.7) is employed on a hyperbolic region of the complex Euclidean plane where $\mathrm{Re}(k^2) \geqslant -\frac{1}{4}m_\phi^2$ and m_ϕ is the mass of the ϕ meson. On this domain, our results indicate that the forms given in Eqs. (3.7) are sufficient to describe the hadron observables considered herein.

The inverse propagator of a quark with flavor f is defined in terms of the two functions $A_f(k^2)$ and $B_f(k^2)$ as given by Eq. (3.6). These are obtained from $\sigma_V^f(k^2)$ and $\sigma_S^f(k^2)$ by inverting Eq. (3.5). In Fig. 3, the functions $A_u(k^2)$ and $B_u(k^2)$ that correspond to the confined u-quark propagator are shown in order to illustrate some of their features, which play an important role in this work.

In the limit that the quark momentum k^2 becomes large and spacelike, the functions $A_f(k^2)$ and $B_f(k^2)$ approach an asymptotic limit:

$$\lim_{k^2\to\infty} \quad A_f(k^2) = 1, \tag{3.8}$$

$$\lim_{k^2\to\infty} \quad B_f(k^2) = m_f. \tag{3.9}$$

Hence, the confined-quark propagator $S_f(k)$ reduces to a free-fermion propagator:

$$\lim_{k^2\to\infty} \quad S_f^{-1}(k) = i\gamma\cdot k + m_f. \tag{3.10}$$

This behavior can be identified with the asymptotic freedom of the quark propagator in QCD.

For small quark momenta, the quark propagator, given by Eqs. (3.7), behaves quite differently than the free-fermion propagator of Eq. (3.10). In this region, there is a strong nonperturbative enhancement of the mass function $B_f(k^2)$. This enhancement is a manifestation of dynamical chiral symmetry breaking and confinement.

Dynamical chiral symmetry breaking causes the low-momentum quark propagator to behave qualitatively as a constituent-quark propagator. [A constituent-quark propagator is given by the free-fermion propagator of Eq. (3.10), but with a mass of the order of a hadron mass.] One can identify an *effective* constituent-quark mass[1] for the confined-quark propagator given in Eqs. (3.7) as the solution of $k^2 - B_f(k^2)/A_f(k^2) = 0$. With this definition, we find the effective u-quark mass is $M_Q^u \approx$ 330 MeV and the effective s-quark mass is $M_Q^s \approx$ 490 MeV. These masses are typical of the values employed in constituent-quark models. The fact that the quark propagator of Eqs. (3.7) behaves as a constituent-quark propagator at low momentum and a current-quark propagator at high momentum has important ramifications in our analysis of vector-meson electroproduction in Sec. IV.

We now consider the Bethe-Salpeter amplitude $\Gamma_\pi(k)$. In the limit $m_u \to 0$ the π meson can be identified with the Goldstone mode of massless QCD and one can show that the corresponding BS equation coincides with DSE for the quark mass function $B_u(k^2)$ [28]. Therefore, the pion BS amplitude can be written as

$$\Gamma_\pi(k) = i\gamma_5 \frac{B_u(k^2)}{f_\pi}\bigg|_{m_u=0}, \tag{3.11}$$

where $B_u(k^2)$ is given by Eq. (3.6) and f_π is the BS normalization. Explicit chiral symmetry breaking effects associated with finite current-quark mass are provided for by allowing $C^u_{m_u=0} = 0$ in Table I, then the small value of $C^u_{m_u=0}$ obtained in Ref. [12] and given in Table I suggests that the π meson is, to a good approximation, a Goldstone mode of QCD.

Using the confined-quark propagator $S_f(k)$ with Eqs. (3.7), π-meson BS amplitude $\Gamma_\pi(k)$ in Eq. (3.11), the quark-loop integrations of Eqs. (3.3) and (3.4) are evaluated numerically. The πN elastic scattering differential cross section is then obtained from

$$\frac{d\sigma}{dt} = \frac{M_N^2}{16\pi s|\vec{p}_{\mathrm{c.m.}}|^2}\frac{1}{2}\sum_{m,m'}|T_{\pi N\to\pi N}|^2. \tag{3.12}$$

The parameters β_u and α_1 are chosen to provide the best agreement with existing πN elastic scattering data in the high-energy and small-momentum-transfer region. The resulting parameters are given in the first row of Table II. The results (solid curves) and the data at $\sqrt{s} =$ 10, 15, and 20 GeV are shown in Fig. 4. Clearly, the model provides a good description of the πN differential cross section.

To determine the remaining parameter β_s we apply our model interaction to KN elastic scattering. The K^+N elastic scattering amplitude can be obtained from Eq. (3.1) by mak-

[1]The reader is reminded that a confined-quark propagator does not have a well-defined mass. Hence, the procedure employed to define an ''effective mass'' is arbitrary.

TABLE II. Parameters of the quark-nucleon Pomeron-exchange interaction of Eq. (2.6). Entry of ''same'' indicates that value is the same as for u and d quarks.

flavor	α_0	α_1 [GeV^{-2}]	β_f [GeV^{-2}]
u/d	0.10	0.33	2.35
s	same	same	1.50
c	0.42	0.10	0.09

ing the substitution $\pi \to K$ and using Eqs. (3.3) and (3.4) with the substitutions $\pi \to K$ and $d \to s$. The amplitude can be calculated immediately by employing the s-quark propagator of Eqs. (3.7), the s-quark parameters given in Table I, and the K-meson BS amplitude $\Gamma_K(k)$ determined from Eq. (3.11) with the replacements $\pi \to K$ and $u \to s$.

We find that the *magnitude* of the KN elastic scattering data can be best reproduced by choosing $\beta_s = 1.5$ GeV^{-1}, as listed in Table II. Our results for $\sqrt{s} = 10$,15, and 20 GeV are shown in Fig. 5. The agreement with the data is excellent. We emphasize that the t dependence of the differential cross section shown in Fig. 5 is a *prediction* of the model since all of the s and t dependence of the quark-nucleon Pomeron-exchange interaction has been fixed by the πN elastic scattering data. Our results for the differential cross section, shown in Figs. 4 and 5, are well parametrized by the form

$$\frac{d\sigma}{dt} = Ae^{bt}, \tag{3.13}$$

where A and b are functions of s only. A determination of $b_{\pi N}$ and b_{KN} from our model reveals that although our quark-nucleon Pomeron-exchange interaction $G(s,t)$ in Eq. (2.5) has the same t dependence for both of these processes, nonetheless, because of the quark-loop integration in Eqs. (3.3) and (3.4), $b_{\pi N} \neq b_{KN}$. In particular, we find that at $\sqrt{s} = 15$ GeV, $b_{\pi N} = 9.17$ GeV^{-2}, and $b_{KN} = 8.82$ GeV^{-2}. This flavor dependence of the t-slope parameter arises from the dynamical difference between the quark substructure of the π and K meson. The only other source of flavor dependence in our approach is the coupling *constant* β_f which is independent of s and t. This illustrates how flavor dependence in diffractive processes can arise from the quark substructure of the hadrons involved. In the next section, we show that the different quark substructure of the ρ, ϕ, and J/ψ mesons leads to striking differences in the q^2 dependence of their electroproduction cross sections.

Having defined all of the parameters in the quark-nucleon Pomeron-exchange interaction of Eqs. (2.5) and (2.6), we are now in a position to make parameter-free predictions for other diffractive processes on a nucleon target.

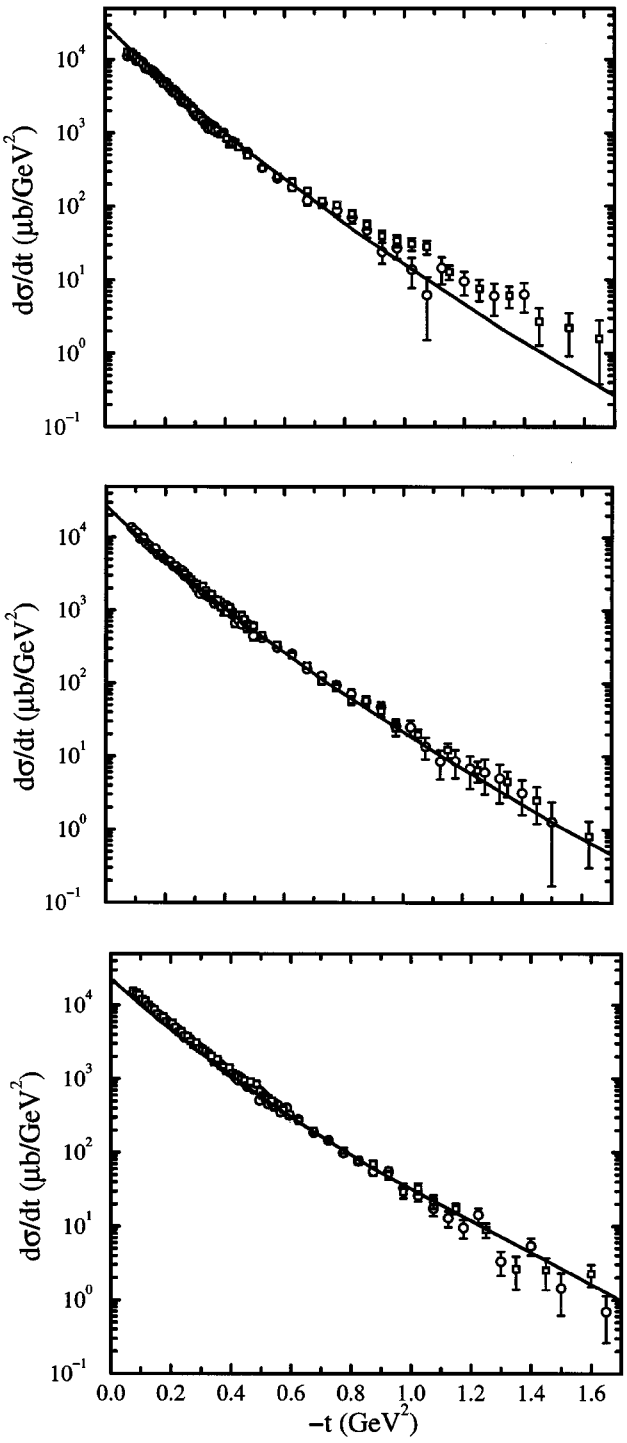

FIG. 4. The differential cross section for πp elastic scattering at c.m. energies $\sqrt{s} =$ 20 (top), 15 (middle) and 10 GeV (bottom). The data are from Ref. [29]. Both $\pi^+ p$ (circles) and $\pi^- p$ (squares) data are shown.

IV. DIFFRACTIVE ELECTROPRODUCTION OF VECTOR MESONS

Motivated by recent experimental efforts at HERA, Fermilab, and TJNAF, the remainder of this paper focuses on the diffractive electroproduction of vector mesons on the nucleon. Our main objective is to explore the role played by the quark substructure of vector mesons in diffractive electroproduction. We also examine the extent to which the quark-nucleon Pomeron-exchange interaction defined by Eq. (2.6) can account for the existing data and make predictions for future experiments.

To proceed, it is necessary to develop model quark-antiquark BS amplitudes for the vector mesons under consideration. In principle, one could solve the BS equation directly to obtain these amplitudes. However, for our present purposes, it is sufficient to construct phenomenological amplitudes that reproduce the experimental decay widths of the

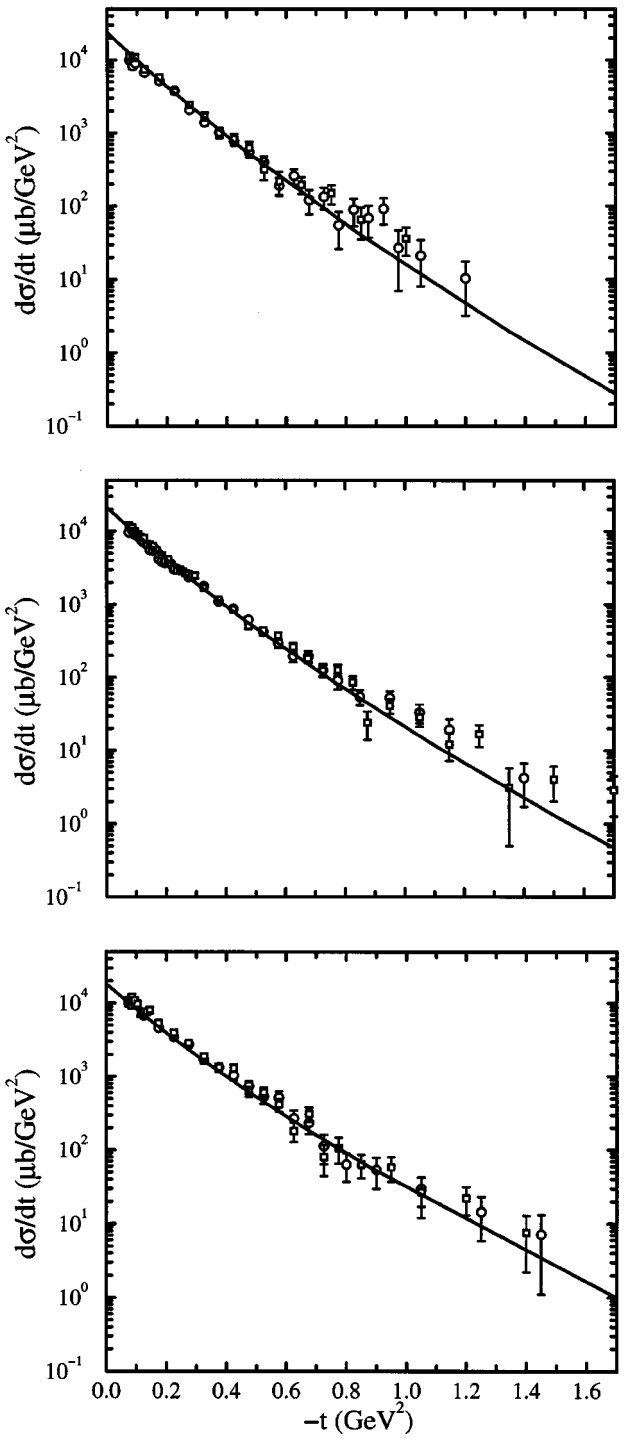

FIG. 5. The differential cross section for Kp elastic scattering at c.m. energies $\sqrt{s}=$ 20 (top), 15 (middle), and 10 GeV (bottom). The data are from Ref. [29]. Both K^+p (circles) and K^-p (squares) data are shown.

vector mesons. In what follows, only formulas necessary to the calculation of ρ decays are given. By making an appropriate change of labels, the same formulas can be applied to calculate the decays of ϕ and J/ψ mesons.

The vector-meson BS amplitudes obtained in numerical DSE studies of the meson spectrum indicate that the qualitative features of these amplitudes are finite at $k^2=0$ and evolve as $1/k^2$ for large k^2 [30]. Therefore, we parametrize the amplitudes

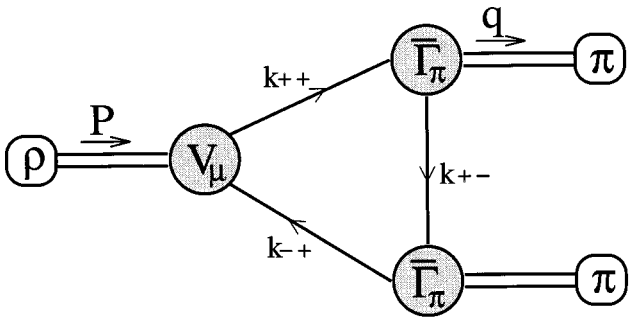

FIG. 6. Impulse approximation to $\rho\to\pi\pi$ decay.

$$V_\mu(p,p')=\frac{1}{N_V}\left(e^{-k^2/a_V^2}+\frac{c_V}{1+k^2/b_V^2}\right)\left[\gamma_\mu+\frac{P_\mu\gamma\cdot P}{m_V^2}\right], \tag{4.1}$$

where $P=p-p'$ and m_V are the total momentum and mass of the vector meson and $k=\frac{1}{2}(p+p')$ is the relative momentum between the quark and antiquark. The parameters a_V, b_V, and c_V represent, respectively, the infrared scale, the scale of the $1/k^2$ tail, and their relative strength. The overall normalization N_V is *not* a free parameter. It is determined by the BS normalization equation

$$\begin{aligned}P_\alpha&\left(\delta_{\mu\nu}+\frac{P_\mu P_\nu}{m_\rho^2}\right)\\&=N_c\mathrm{tr}\int\frac{d^4k}{(2\pi)^4}\frac{\partial S_u(k_+)}{\partial P_\alpha}V_\mu(k_+,k_-)S_u(k_-)V_\nu(k_-,k_+)\\&\quad+N_c\mathrm{tr}\int\frac{d^4k}{(2\pi)^4}S_u(k_+)V_\mu(k_+,k_-)\\&\quad\times\frac{\partial S_u(k_-)}{\partial P_\alpha}V_\nu(k_-,k_+).\end{aligned} \tag{4.2}$$

The Dirac structure of the BS amplitude in Eq. (4.1) is not the most general form. Rather, it is the simplest form to ensure that the *Lorentz condition* is satisfied by the on-mass-shell vector meson; i.e., $P_\mu V_\mu(p,p')=0$.

To determine the parameters in $V_\mu(p,p')$, we first consider the decay of a neutral-ρ meson of momentum P into a π^+ meson of momentum q and a π^- meson of momentum $q'=P-q$. In impulse approximation, the $\rho\to\pi\pi$ transition amplitude is

$$\langle q;P-q|T_{\rho\to\pi\pi}|P\lambda_\rho\rangle=-2\Lambda_\mu(P,q)\varepsilon_\mu^{\lambda_\rho}(P), \tag{4.3}$$

where $\varepsilon_\mu^{\lambda_\rho}(P)$ is the polarization vector of a ρ meson with helicity λ_ρ and

$$\begin{aligned}\Lambda_\mu(P,q)=2N_c\mathrm{tr}&\int\frac{d^4k}{(2\pi)^4}S_u(k_{-+})V_\mu(k_{-+},k_{++})\\&\times S_u(k_{++})\overline{\Gamma}_\pi(k+\tfrac{1}{2}P)S_d(k_{+-})\overline{\Gamma}_\pi(k).\end{aligned} \tag{4.4}$$

Here, $k_{\alpha\beta}=k+(\alpha/2)P+(\beta/2)q$, $N_c=3$, and the trace is over Dirac indices. The Feynman diagram corresponding to Eq. (4.4) is depicted in Fig. 6. Since the quark propagator $S_f(k)$ and π-meson BS amplitude $\Gamma_\pi(k)$ have been given in

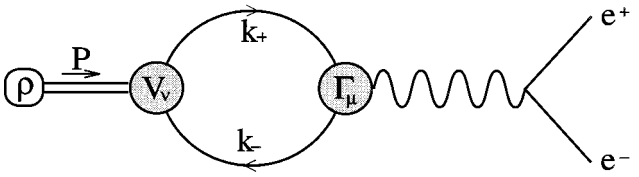

FIG. 7. Impulse approximation to $\rho\to e^+e^-$ decay.

the previous section, the only new element in Eq. (4.4) is the ρ-meson BS amplitude $V_\mu(p,p')$. Therefore, Eq. (4.4) provides a means to determine the parameters a_ρ, b_ρ, and c_ρ in the ρ-meson BS amplitude $V_\mu(p,p')$.

We define the $\rho\to\pi\pi$ decay constant $g_{\rho\pi\pi}$ by writing Eq. (4.4) as

$$\Lambda_\mu(P,q)=\tfrac{1}{4}(2q_\mu-P_\mu)g_{\rho\pi\pi}\Lambda(P^2,q^2), \tag{4.5}$$

with $\Lambda(P^2=-m_\rho^2,q^2=-m_\pi^2)=1$ when all external legs of Fig. 6 are on-mass-shell. The $\rho\to\pi\pi$ decay width $\Gamma_{\rho\to\pi\pi}$ is related to this decay constant by the expression

$$\Gamma_{\rho\to\pi\pi}=\frac{g_{\rho\pi\pi}^2}{4\pi}\frac{m_\rho}{12}\left(1-\frac{4m_\pi^2}{m_\rho^2}\right)^{3/2}. \tag{4.6}$$

Substituting the experimental value of $\Gamma_{\rho\to\pi\pi}=151.2\pm 1.2$ MeV [31] into Eq. (4.6) leads to $g_{\rho\pi\pi}=6.05$. Upon substituting the explicit form for $V_\mu(p,p')$ into Eq. (4.4), we determine the value of the decay constant $g_{\rho\pi\pi}$ in our model.

We also consider the ρ-meson electromagnetic decay $\rho\to e^+e^-$ which proceeds through an intermediate timelike photon. The transition amplitude for the decay of a ρ meson with momentum P into an electron of momentum p and a positron of momentum p' takes the form

$$\langle pm_s;p'm_s'|T_{\rho\to e^+e^-}|P\lambda_\rho\rangle$$
$$=e_0\overline{u}_{m_s}(p)\gamma_\mu v_{m_s'}(p')\frac{1}{P^2}\Pi_{\mu\nu}(P)\varepsilon_\nu^{\lambda_\rho}(P), \tag{4.7}$$

where $\overline{u}_{m_s}(p)$ and $v_{m_s'}(p')$ are, respectively, the spinors of the outgoing electron and positron, e_0 is the positron charge, $\Pi_{\mu\nu}(P)$ is the photon-ρ-meson transition amplitude, and $\varepsilon_\nu^{\lambda_\rho}(p)$ is the ρ-meson polarization vector. In impulse approximation, the photon-ρ-meson transition amplitude is given by

$$\Pi_{\mu\nu}(P)=e_0N_c\mathrm{tr}\int\frac{d^4k}{(2\pi)^4}S_u(k_+)\Gamma_\mu(k_+,k_-)S_u(k_-)$$
$$\times V_\nu(k_-,k_+), \tag{4.8}$$

and is illustrated in Fig. 7.

Evaluation of Eq. (4.8) requires an explicit form for the photon-quark vertex $\Gamma_\mu(k,k')$. An acceptable form must satisfy the Ward-Takahashi identity (WTI):

$$(k-k')_\mu i\Gamma_\mu(k,k')=S_f^{-1}(k)-S_f^{-1}(k'), \tag{4.9}$$

where $S_f(k)$ is the quark propagator. Clearly, a bare quark-photon vertex $\Gamma_\mu=\gamma_\mu$ does not satisfy Eq. (4.9) for the confined-quark propagators of Eqs. (3.7).

The most general quark-photon vertex that satisfies Eq. (4.9) and is free of kinematic singularities is given by [32]

$$i\Gamma_\mu(k,k')=i\Gamma_\mu^{\mathrm{T}}(k,k')+i\Gamma_\mu^{\mathrm{BC}}(k,k'), \tag{4.10}$$

where

$$(k-k')_\mu\Gamma_\mu^{\mathrm{T}}(k,k')=0, \tag{4.11}$$

and [33]

$$i\Gamma_\mu^{\mathrm{BC}}(k,k')=i\gamma_\mu f_1(k^2,k'^2)+(k+k')_\mu\left[i\gamma\cdot\frac{k+k'}{2}\right.$$
$$\left.\times f_2(k^2,k'^2)+f_3(k^2,k'^2)\right], \tag{4.12}$$

with

$$f_1(k^2,k'^2)=\frac{A_f(k^2)+A_f(k'^2)}{2},$$
$$f_2(k^2,k'^2)=\frac{A_f(k^2)-A_f(k'^2)}{k^2-k'^2},$$
$$f_3(k^2,k'^2)=\frac{B_f(k^2)-B_f(k'^2)}{k^2-k'^2}. \tag{4.13}$$

The functions $A_f(k^2)$ and $B_f(k^2)$ are the Lorentz invariant functions that determine the inverse of the confined-quark propagator in Eq. (3.6).

We observe from Eqs. (4.12) and (4.13) that $\Gamma_\mu^{\mathrm{BC}}(k,k')$ reduces to a bare quark-photon vertex γ_μ in the limit that both quark momenta become large and spacelike, in accordance with perturbative QCD. Hence, in this perturbative limit, $\Gamma_\mu^{\mathrm{T}}(k,k')$ must vanish. Of course, at $q=k-k'=0$ the Ward identity fixes the full quark-photon vertex to be equal to $\Gamma_\mu^{\mathrm{BC}}(k,k)$, therefore, in this limit $\Gamma_\mu^{\mathrm{T}}(k,k)$ must also vanish. Furthermore, numerical studies indicate that in the spacelike region, $\Gamma_\mu^{\mathrm{T}}(k,k')$ is a slowly varying function of photon momentum. With these considerations, it is reasonable to neglect contributions to the quark-photon vertex from $\Gamma_\mu^{\mathrm{T}}(k,k')$. So, throughout this work we use

$$\Gamma_\mu(k,k')=\Gamma_\mu^{\mathrm{BC}}(k,k'). \tag{4.14}$$

This ensures that we have a parameter-free quark-photon vertex that satisfies the WTI and has the correct perturbative limit as both k^2 and k'^2 become large and spacelike. Furthermore, it has the correct transformation properties under C, P, T, and Lorentz transformations.

Since the ρ meson is on-mass-shell, $\Pi_{\mu\nu}(P)$ is transverse to P_μ. We can, therefore, define the dimensionless ρ-meson electromagnetic decay constant f_ρ by

$$\Pi_{\mu\nu}(P)\Big|_{P^2=-m_\rho^2}=(P^2\delta_{\mu\nu}+P_\mu P_\nu)\frac{e_0}{f_\rho}\Big|_{P^2=-m_\rho^2}. \tag{4.15}$$

One can then show that the decay width for $\rho\to e^+e^-$ is given by

TABLE III. Parameters of the model vector-meson BS amplitudes and their corresponding decay constants. VPP refers to the vector-meson decay into two pseudoscalar mesons, e.g., $\rho\to\pi\pi$ and $\phi\to K\overline{K}$. The experimental values are given in parentheses.

V meson	a_V (GeV)	b_V (GeV)	c_V	f_V	g_{VPP}
ρ	0.400	0.008	125.0	4.55 (5.03)	6.8 (6.05)
ϕ	0.450	0.400	0.5	14.8 (12.9)	3.7 (4.55)
J/ψ	1.200		0.0	11.5 (11.5)	

$$\Gamma_{\rho\to e^+e^-}=\frac{1}{3}\alpha_{\rm em}^2 m_\rho\frac{4\pi}{f_\rho^2}, \tag{4.16}$$

where $\alpha_{\rm em}\equiv e_0^2/4\pi\approx 1/137$ is the fine structure constant of QED. The experimental value of $\Gamma_{\rho\to e^+e^-}=6.77\pm 0.32$ keV [31] entails $f_\rho=5.03$.

With the above formulas, we can use the experimental data of the $\rho\to\pi\pi$ and $\rho\to e^+e^-$ decay widths to constrain the parameters of the ρ-meson BS amplitude $V_\mu(p,p')$. The parameters a_ρ, b_ρ, and c_ρ are chosen to reproduce the experimental values of the decay constants f_ρ and $g_{\rho\pi\pi}$ to within 15% of the experimental values. This accuracy is easily acheived with our simple model of the vector-meson BS amplitude. Furthermore, our results for the W, t, and q^2 dependence of vector-meson electroproduction observables are completely insensitive to changes made to the parameters of the BS amplitude. Only the magnitudes of decay constants and the electroproduction cross section are sensitive to changes in the model BS amplitude. The chosen parameters for the ρ-meson BS amplitude and the resulting decay constants are compared to the experimental values for the decay constants in the first row of Table III.

Relabeling $\rho\to\phi$ and $u\to s$ in Eqs. (4.8) and (4.16) and $\rho\to\phi$, $\pi\to K$, and $u\to s$ in Eqs. (4.4), (4.5), and (4.6) and multiplying Eq. (4.8) by $\sqrt{2/9}$ to take account of the flavor structure of the ϕ meson, one can determine the BS amplitude for the ϕ meson by reproducing the decay constants for $\phi\to\overline{K}K$ and $\phi\to e^+e^-$. The resulting parameters and decay constants are given in Table III.

Having completed the determination of the necessary BS amplitudes, we can now predict diffractive, ρ- and ϕ-meson electroproduction cross sections. This is carried out in the next sections.

A. Electroproduction of ρ mesons

The fact that a neutral vector meson and photon are both $J^{PC}=1^{--}$ states suggests that diffractive vector-meson electroproduction would be similar to elastic hadron scattering, in that both processes satisfy the empirical rule of Gribov and Morrison (see, for example, Ref. [1]). We therefore expect that diffractive electroproduction of neutral vector mesons would be well described within our Pomeron-exchange model. The first application of a quark-based Pomeron-exchange model to the study of vector-meson electroproduction is given in Ref. [6].

We argue that of the processes considered herein, vector-meson electroproduction is *most* sensitive to the quark substructure of mesons and a proper treatment of the confined-quark dynamics is essential to obtain a description of vector-meson electroproduction. For example, when we neglect some of the nonperturbative aspects of quark propagation, such as confinement and dynamical chiral symmetry breaking, we find that agreement with electroproduction data requires the inclusion of a quark-Pomeron-exchange form factor [8]. In contrast to this, herein, we observe that the *same* quark-nucleon Pomeron-exchange interaction that describes πN and KN elastic scattering also provides an excellent description of ρ- and ϕ-meson electroproduction without changing any parameters and without introducing a quark-Pomeron form factor.

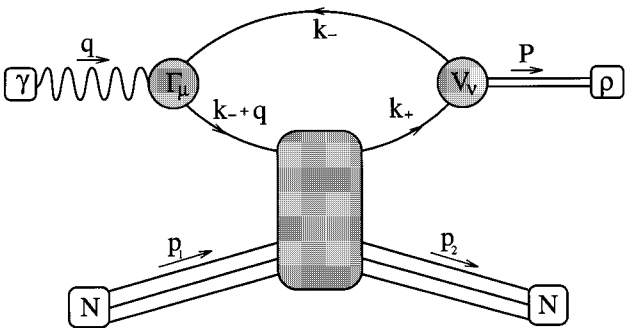

FIG. 8. Impulse approximation to ρ-meson electroproduction current matrix element, Eq. (4.19) with $t_{\mu\alpha\nu}(q,P)$ from Eq. (4.20).

The differential cross section for vector-meson electroproduction can be written as

$$\frac{d\sigma}{dE_{e'}d\Omega_{e'}}=\Gamma(\sigma_T+\epsilon\sigma_L). \tag{4.17}$$

Here, we have introduced the lepton kinematical factors Γ and ϵ as in Ref. [34]. The definitions of σ_T and σ_L admit their identification as the *transverse* and *longitudinal* cross sections of the *virtual* process $\gamma^*N\to\rho^0N$.

The differential forms of σ_T and σ_L, in the center-of-momentum (c.m.) frame of the ρN system, can be written as

$$\frac{d\sigma_T}{d\Omega}=\frac{1}{(2\pi)^2}\frac{M_N}{4W}\frac{|\vec{P}|}{K_H}\frac{1}{2}\sum_{\rm spins}(J_xJ_x^\dagger+J_yJ_y^\dagger),$$

$$\frac{d\sigma_L}{d\Omega}=\frac{1}{(2\pi)^2}\frac{M_N}{4W}\frac{|\vec{P}|}{K_H}\frac{q^2}{\omega^2}\sum_{\rm spins}(J_zJ_z^\dagger). \tag{4.18}$$

Here, $d\Omega$ denotes a differential element of the solid angle of the outgoing ρ-meson three-momentum $\vec{P}$ relative to the photon three-momentum $\vec{q}$, $K_H=(W^2-M_N^2)/(2M_N)$, $W^2=-(P+p_2)^2$ is the invariant mass of the ρN system, $q_\mu=(\vec{q},i\omega)$ is the momentum of the virtual photon, and $P_\mu=(\vec{P},i\sqrt{m_\rho^2+|\vec{P}|^2})$ is momentum of the outgoing ρ meson. The hadron current matrix element is $J_\mu=\langle P\lambda_\rho;p_2m'|J_\mu(q)|p_1m\rangle$.

Application of the quark-nucleon Pomeron-exchange interaction, defined in Eq. (2.6), to ρ-meson electroproduction leads to the diagram illustrated in Fig. 8. The corresponding current matrix element is

$$\langle P\lambda_\rho; p_2 m' | J_\mu(q) | p_1 m\rangle$$
$$= 2 t_{\mu\alpha\nu}(q,P)\ \varepsilon_\nu^{\lambda_\rho}(P)[G(w^2,t)\ \ 3\beta_u F_1(t)]$$
$$\times[\overline{u}_{m'}(p_2)\gamma_\alpha u_m(p_1)]. \quad (4.19)$$

Here, $u_m(p_1)$ and $\overline{u}_{m'}(p_2)$ are, respectively, the spinors for the incoming and outgoing nucleon, $t=-(p_1-p_2)^2\leq 0$; $\varepsilon_\nu^{\lambda_\rho}(P)$ is the polarization vector of the ρ meson, and the factor of 2 arises from the equivalence of the two contributing diagrams under charge conjugation because the quark-Pomeron-exchange vertex is even under charge conjugation. The Pomeron-exchange parametrization $G(w^2,t)\ 3\beta_u F_1(t)$ has been defined in Eqs. (2.5) and (2.6). The energy of the quark-nucleon Pomeron-exchange interaction is taken to be $w^2=-(q+\frac{1}{2}P+p_1)^2$, which follows from the observation that the quark-loop integration is sharply peaked about a momentum for which the vector-meson BS amplitude takes its maximum value. This approximation ensures that $t_{\mu\alpha\nu}(q,P)$ is a function of q and P only, thereby allowing one of the four integrations necessary in calculating $t_{\mu\alpha\nu}(q,P)$ to be carried out analytically. We have investigated the ramifications of this approximation and find that the W, t, and q^2 dependences of the observables considered herein are insensitive to it and that the magnitudes of cross section are insensitive to within 10%.

The amplitude $t_{\mu\alpha\nu}(q,P)$ in Eq. (4.19), describes the coupling of the photon and ρ meson to the nucleon via Pomeron exchange. It is analogous to $\Lambda_\mu(q,P)$ in Eq. (3.1) for meson-nucleon elastic scattering. In impulse approximation, $t_{\mu\alpha\nu}(q,P)$ is given by

$$t_{\mu\alpha\nu}(q,P)=\beta_u N_c e_0 \mathrm{tr}\int \frac{\mathrm{d}^4k}{(2\pi)^4} S_u(k_-)\Gamma_\mu(k_-,k_-+q)$$
$$\times S_u(k_-+q)\gamma_\alpha S_u(k_+)V_\nu(k_+,k_-), \quad (4.20)$$

where $k_\alpha=k+(\alpha/2)P$, $N_c=3$, $e_0=\sqrt{4\pi\alpha_{\mathrm{EM}}}$, and β_u is given in Table II. All of the elements in Eq. (4.20) have been determined in previous sections, hence, there are *no* free parameters in our calculation of vector-meson electroproduction. We now present the results of our model and compare them to the data.

We first consider the differential cross section for ρ-meson photoproduction at $W=$ 80 GeV. Our prediction is the solid curve shown in Fig. 9. Both the magnitude and t dependence are in excellent agreement with the data. In Fig. 9, we also show the result (dashed curve) from Ref. [8], obtained using the model parameter $\alpha_1=$ 0.25 GeV^{-2}, which was taken directly from Ref. [6] and therefore, is *not* a self consistent determination within our model. In the present work, the value $\alpha_1=$ 0.33 GeV^{-2} is determined by the t dependence of πN elastic scattering as discussed in Sec. III A. Upon comparing the solid and dashed curves in Fig. 9, we observe that our new calculated value of $\alpha_1=0.33$ GeV^{-2} has improved the agreement with data, especially at small t. This illustrates the importance of using a value of α_1 that is consistent with our confined-quark propagators and BS amplitudes.

We now consider the q^2 dependence of the ρ-meson electroproduction cross section. This is the most important result

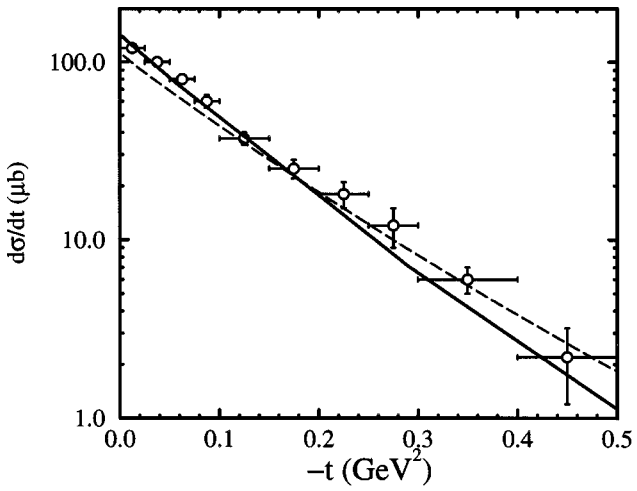

FIG. 9. Our results for the differential cross section for ρ-meson photoproduction ($q^2=0$) at $W=80$ GeV. The solid curve is the prediction of the present study and the dashed curve is the result from Ref. [8]. The data are from Ref. [35].

obtained in this work. Our model elucidates the relation between the q^2 dependence of the electroproduction cross section and the quark substructure of the vector meson. At present, the origin of the q^2 dependence of diffractive electroproduction is still under debate. We show here that, in our model, it arises *entirely* from the quark substructure of the vector meson.

In Fig. 10, the predicted q^2 dependence of the total cross section is compared with the data. Our prediction for $W=15$ GeV and $\epsilon=0.5$ is shown as the solid curve in Fig. 10. The agreement with the data is excellent. We emphasize that *no* parameters were varied to achieve this result. Such excellent agreement is unique to this model.

Before we consider other electroproduction observables, let us illustrate some of the dynamics that gives rise to the

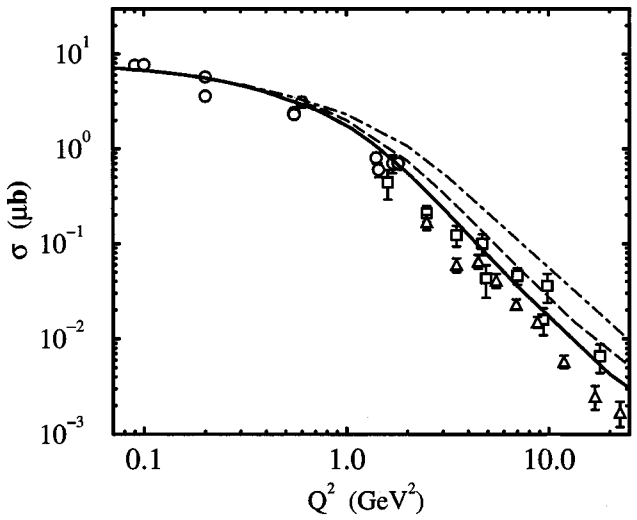

FIG. 10. The q^2 dependence of the neutral ρ-meson electroproduction cross section at $W=$ 15 GeV. The solid curve is the result of our model. The data are from Ref. [36] (circles), Ref. [37] (squares), and Ref. [38] (triangles). The dashed and dot-dashed curves are the cross sections obtained from our model, but with current-quark masses of 10 and 25 times greater than that given for m_u in Table I.

predicted q^2 dependence of the ρ-meson electroproduction cross section (solid curve) shown in Fig. 10. First, we observe that our prediction exhibits different behaviors in the low-q^2 and high-q^2 region. For $q^2 < 1\ \mathrm{GeV}^2$, the cross section falls off slowly with q^2, while for $q^2 > 1\ \mathrm{GeV}^2$, it falls off more rapidly and can be parametrized by the form

$$\sigma(W=15\ \mathrm{GeV}, q^2>1\ \mathrm{GeV}^2) = \sigma_0 \left(\frac{q^2}{1\ \mathrm{GeV}^2} \right)^{a/2}, \tag{4.21}$$

with $\sigma_0 = 2.047\ \mu b$, and $a = -4.070$, so that $\sigma(q^2 > 1\ \mathrm{GeV}^2) \propto 1/q^4$. This value of a is in good agreement with those obtained by experiment: $a = -3.96 \pm 0.36$ from Ref. [37], $a = -4.10 \pm 0.18$ from Ref. [38], and $a = -4.2 \pm 0.8$ from Ref. [39]. Theoretical predictions of a in models that employ perturbative methods typically find values in the range $a = -6$ [18] and $a \approx -4.8$ [22].

The dynamical origin of the $1/q^4$ dependence in our model can be understood from the following considerations. The domain of the integration momentum sampled in Eq. (4.20) is principally determined by the BS amplitude of the ρ meson. This is because the BS amplitude provides most of the damping to the integrand. Therefore, the integrand is sharply peaked at $k^2 \approx 0$, where the ρ-meson BS amplitude has its maximum value. The integration can be approximated by evaluating the integrand at $k^2 = 0$, in which case we find that the photon momentum q is primarily concentrated in *one* of the quark propagators. (This was also observed in Ref. [6].) This quark propagator results in a $1/q^2$ dependence in Eq. (4.20) for large q^2. Since the cross section is proportional to the square of the hadron current (4.19), we have

$$\sigma(W, q^2 \gg q_0^2) \propto \frac{1}{1 + [q^2/(q_0^2)_\rho]^2}, \tag{4.22}$$

where $(q_0^2)_\rho$ is a scale that determines the onset of the $1/q^4$ behavior. This argument is independent of the flavor of the quark or the particular vector meson under consideration. It arises solely from the quark loop in Eq. (4.20) and the fact that the vector meson is a bound state with a BS amplitude peaked at zero quark-antiquark relative momentum.

The value of q^2, at which the transition to the $1/q^4$ behavior occurs, depends on the scale $(q_0^2)_\rho$ which, in turn, depends on the current-quark mass m_f. To illustrate this, we allow the current-quark mass in the quark propagator $S_u(k)$ to take on values 10 and 25 times larger than the value of $m_u = 5.1$ MeV, given in Table I. To remain self-consistent, we recalculate the parameters a_ρ and b_ρ of the ρ-meson BS amplitude in Eq. (4.1) in order to maintain the values of the decay constants f_ρ and $g_{\rho\pi\pi}$ in Table III. The dashed (dot-dashed) curve shown in Fig. 10 is our prediction of the ρ-meson electroproduction cross section with a current u-quark mass 10 (25) times larger than $m_u = 5.1$ MeV.

We observe that all three curves in Fig. 10 converge to the same value at $q^2 = 0$. This is due to the fact that our dressed quark-photon vertex $\Gamma_\mu^{\mathrm{BC}}(k,k')$ satisfies the WTI and the Ward identity. The Ward identity places very tight constraints on the behavior of the cross section at $q^2 = 0$. This feature is also observed in studies of π-meson observables where the unit normalization of the EM form factor arises from the close connection between the normalization of the pion BS amplitude and the Ward identity [13].

We also observe that for large values of q^2, all three curves in Fig. 10 exhibit the *same* $1/q^4$ falloff. This $1/q^4$ behavior at high q^2 is a general feature of the model, *independent* of the value of m_f. However, the transition from a cross section that slowly decreases with q^2 to one that falls off as $1/q^4$, occurs at a value of $(q_0^2)_\rho$ which *increases* with the current-quark mass m_f. This suggests that the electroproduction cross sections for heavy-quark vector mesons reach this $1/q^4$ falloff at larger values of q^2 than for those of light-quark vector mesons. This feature is illustrated in Secs. IV B and IV C when we consider ϕ- and J/ψ-meson electroproduction.

This dependence on the quark mass is a result of having explicitly carried out the quark-loop integration of Eq. (4.20). In studies that do not explicitly carry out the quark-loop integration, it is necessary to introduce a quark-Pomeron-exchange form factor in order to account for the q^2 dependence of the vector meson electroproduction cross section [6,7]. The introduction of this form factor destroys the relationship between the scale of the transition $(q_0^2)_\rho$ and the current-quark mass m_f. Furthermore, the value of $(q_0^2)_\rho$ depends on the quark flavor (since it depends on m_f) which means that the quark-Pomeron-exchange form factor is also flavor *dependent* [7]. Such flavor dependence violates our first assumption in Sec. II and would introduce additional, undetermined parameters in the quark-nucleon Pomeron-exchange interaction. The only flavor dependence in our approach (apart from the constant β_f) arises naturally from the dynamics of the intrinsic quark substructure of the vector meson.

Another important element in the determination of the q^2 dependence of electroproduction is the dressed quark-photon vertex defined by Eq. (4.12). We have already indicated that the value of the diffractive electroproduction cross section, at $q^2 = 0$, is tightly constrained by the fact that the quark-photon vertex employed satisfies the Ward identity. As an estimate of its influence on the electroproduction cross section, we replace the quark-photon vertex $\Gamma_\mu(k,k')$ in Eq. (4.20) with the bare vertex γ_μ. The resulting cross section is shown as a dashed curve in Fig. 11. It can be compared to the full calculation, shown as a solid curve. Clearly, the nonperturbative dressing of the quark-photon vertex is essential in obtaining agreement with data for low q^2, where it contributes significantly to the cross section.

We would like to emphasize that although the effect of nonperturbative contributions to the quark-photon vertex is lessened in the limit $q^2 \to \infty$, it does *not* vanish. It is a misapprehension to expect that at large q^2, the perturbative limit $\Gamma_\mu(k,k') \to \gamma_\mu$ is approached. The quark-photon vertex $\Gamma_\mu(k,k')$ only approaches this perturbative limit when *both* quark momenta become large and spacelike. From the above argument, we know that the quark-loop integration in Eq. (4.20) receives its principal support when $k^2 \approx 0$ and hence one quark propagator carries a large, spacelike momentum $q - \frac{1}{2}P$ (as illustrated by setting $k = 0$ in Fig. 8). However, the other quark propagator, which is attached to the quark-photon vertex, carries momentum $\frac{1}{2}P$: this quark propagator is soft. Consequently, there is *no* value of q^2 for which the

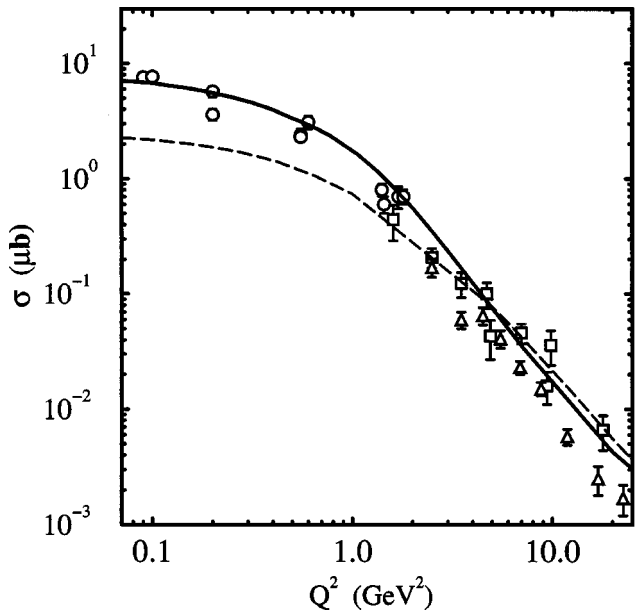

FIG. 11. The effect of dressing the quark-photon vertex on the ρ-meson electroproduction cross section. The solid curve is the result of our model with a dressed quark-photon vertex. The dashed curve is the result of our model with a *bare* quark-photon vertex. The data are the same as in Fig. 10.

quark-photon vertex can be replaced by γ_μ. In the exclusive process of diffractive vector-meson electroproduction, nonperturbative dressing of the quark-photon vertex is always present, at *all* q^2.

It is interesting to note that some observables are particularly sensitive to the nonperturbative dressing of the quark-photon vertex $\Gamma_\mu(k,k')$. As an example of this, in Fig. 12 we show the predicted ratio of the longitudinal and transverse cross sections defined by

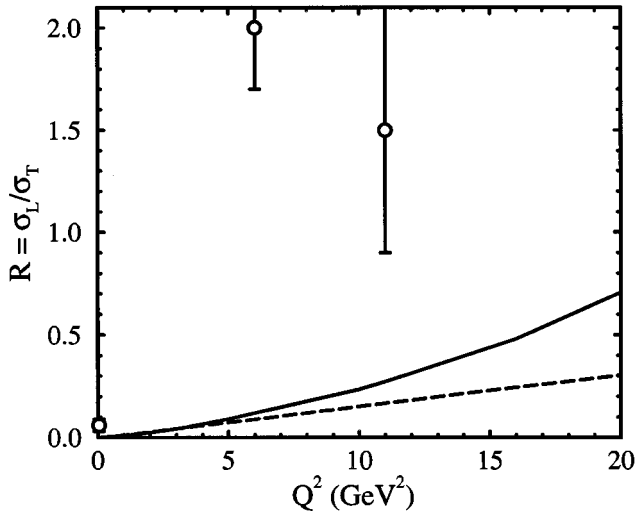

FIG. 12. The q^2 evolution of the ratio of longitudinal to transverse cross sections $R(q^2)$ for ρ-meson electroproduction. The solid curve is the prediction of our model. The dashed line is the prediction of our model with a bare quark-photon vertex γ_μ. The data points are estimated in Ref. [38] and Ref. [40] assuming s-channel helicity conservation.

$$R(q^2)\equiv\frac{\sigma_L}{\sigma_T}. \tag{4.23}$$

This ratio has been examined by previous authors, using both nonperturbative [6] and perturbative models [21]. Their treatment of quark dynamics differ significantly from each other, and from that employed here, they yield results that are consistent with the data shown in Fig. 12.

The result obtained from our model is shown as the solid curve in Fig. 12. The dashed curve is obtained from our model by replacing the dressed vertex with the bare quark-photon vertex γ_μ. We observe that nonperturbative dressing on the quark-photon vertex has a significant effect on $R(q^2)$ for all values of q^2.

A comparison of $R(q^2)$ obtained in our model (solid curve) with the data in Fig. 12, reveals a significant discrepancy. If the discrepancy is real, it might suggest that $R(q^2)$ is sensitive to *transverse* contributions to the dressing of the quark-photon vertex; i.e., to $\Gamma^{\rm T}_\mu(k,k')$. Such contributions have been neglected in this work, as discussed in Sec. III. By comparing the solid and dashed curves of Fig. 12, we observe that $R(q^2)$ is very sensitive to the nonperturbative dressing of the quark-photon vertex. So, although the inclusion of transverse contributions to the quark-photon vertex plays little role in most hadron observables, $R(q^2)$ (a *ratio* of two cross sections, each approaching zero with increasing q^2) may magnify such dynamical effects. This is an intriguing possibility; the ratio $R(q^2)$ may provide a new and important tool with which to investigate the dressing of the quark-photon vertex. Such an investigation is left for future work.

B. Electroproduction of ϕ mesons

The ϕ-meson electroproduction current matrix amplitude is obtained from Eq. (4.19) by relabeling $\rho\to\phi$. The associated amplitude $t^{[\phi]}_{\mu\alpha\nu}(q,P)$ may be obtained from Eq. (4.20) by relabeling $u\to s$ and multiplying by $\sqrt{\frac{2}{9}}$. As in the case of ρ-meson electroproduction, all elements of the calculation have been specified previously. Therefore, there are no free parameters in the application of our model to ϕ-meson electroproduction.

In Fig. 13, we show the ϕ-meson photoproduction differential cross section (lower curve) predicted by our model. It is in good agreement with the recent data. In the same figure, the ρ-meson photoproduction cross section is also displayed for comparison.

The characteristics that distinguish between the quark substructure of the ϕ and ρ mesons can be illustrated by comparing the q^2 dependence of their electroproduction cross sections. The q^2 dependence of the predicted ϕ-meson electroproduction cross section for $W=70$ GeV and $\epsilon=0.5$ is given in Fig. 14 as a solid curve. We have also included our ρ-meson electroproduction results (dashed curve) for comparison. We see that for large values of q^2, the ρ- and ϕ-meson cross sections obey the asymptotic, power law $\approx 1/q^4$. In ϕ-meson electroproduction, the transition to this asymptotic region occurs at $(q_0^2)_\phi\approx 2$ GeV^2. The larger value of $(q_0^2)_\phi$ relative to that of $(q_0^2)_\rho\approx 1$ GeV^2 reflects the difference in magnitude between the relevant scales of the

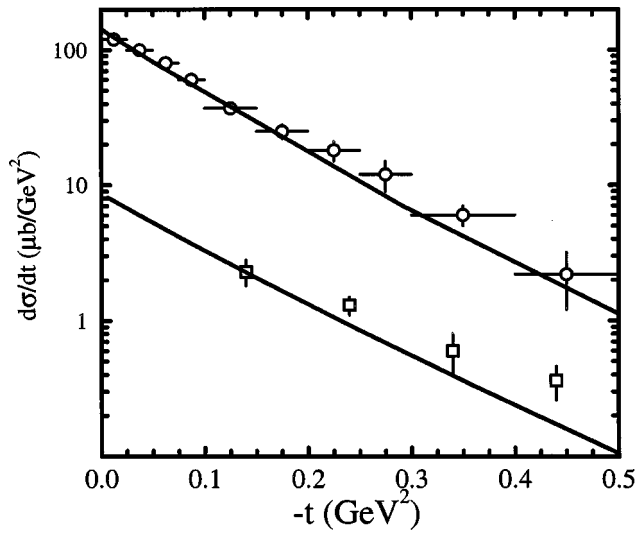

FIG. 13. The differential cross sections for photoproduction ($q^2=0$) of ρ mesons (top curve) and ϕ mesons (bottom curve) at $W=$ 80 GeV. The data are from Refs. [35,41].

u- and s-quark propagators, namely, m_u and m_s. This result was anticipated from our discussion in Sec. IV A. Furthermore, this result entails that for large enough q^2, the ratio of the ρ- and ϕ-meson electroproduction cross sections, $\sigma^{[\rho]}/\sigma^{[\phi]}$ approaches a constant.

While our predictions presented in Fig. 14 are in agreement with the recent data from HERA (circles and triangles), there is a considerable discrepancy between our results and the data reported by the New Muon Collaboration (NMC) (squares) [38]. (The NMC data were measured at the lower energy $W\approx$ 14 GeV. However, the discrepancy between our prediction and the NMC data persists even when the W dependence of our model is accounted for.) The normalization

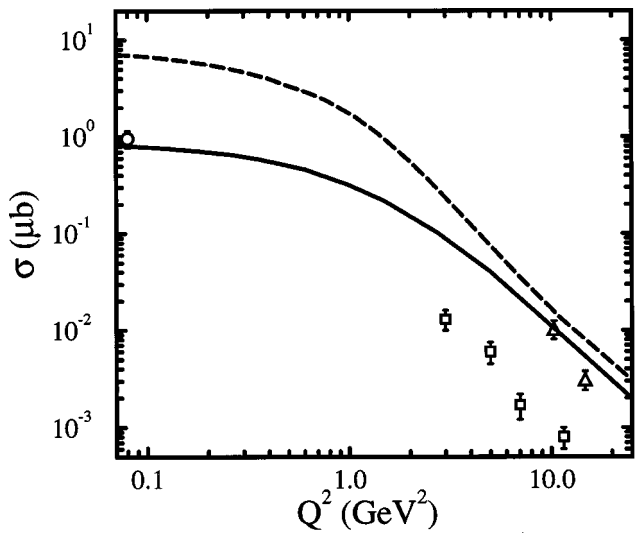

FIG. 14. The solid curve is our prediction for the q^2 dependence of the ϕ-meson electroproduction cross section at $W=$ 70 GeV. The dashed curve is our prediction for the ρ-meson electroproduction cross section at $W=$ 15 GeV, shown here for comparison. The ϕ-meson electroproduction data are from Ref. [42] (triangles) and Ref. [38] (squares). ϕ-meson photoproduction ($q^2=0$) data from Ref. [41] (circles) are also shown at $q^2\approx$ 0.08 GeV^2.

of these data seem abnormally low when compared to the recent data from HERA. This may be due to the fact that these ϕ-meson electroproduction data were obtained by averaging over several *different* nuclear targets (deuterium, carbon, and calcium). If the nuclear effects are not properly accounted for, then a direct comparison of these data to our results on a nucleon target is meaningless. There is evidence from Fermilab experiment E665, that the NMC data for ρ-meson electroproduction may also be low by a factor of 2 [43]. A careful comparison of our prediction for the ρ-meson electroproduction cross section (solid curve in Fig. 10) and the NMC data for this process (triangles in Fig. 10) reveals that these data are a factor of 2 lower than our prediction. We therefore view these data with caution.

It is impossible to reconcile the NMC data for ϕ-meson electroproduction with our model. Agreement with these data requires that the momentum scale $(q_0^2)_\phi$, which determines the onset of the $1/q^4$ falloff for the ϕ-meson electroproduction cross section, would have to be the same as $(q_0^2)_\rho$ for ρ-meson electroproduction. Based on our analysis of the dependence of $(q_0^2)_\rho$ on m_f in Sec. IV A, the requirement that $(q_0^2)_\phi\approx(q_0^2)_\rho$ implies $m_s\approx m_u$. On the contrary, since $m_s\gg m_u$, the ϕ-meson electroproduction cross section should reach the asymptotic $1/q^4$ region *later* than that of the ρ meson. We conclude that the NMC data (triangles) in Fig. 14 is not simply related to ϕ-meson electroproduction on a *nucleon* target, and hence such an interpretation of these data is erroneous.

If these NMC data are truly to be interpreted as a measurement of ρ- and ϕ-meson electroproduction on a *nucleon* then a comparison with recent data from HERA (at higher energy but similar q^2) would entail that, at large q^2, electroproduction cross sections exhibit an energy dependence much stronger than that observed in low-q^2 diffractive processes [40]. However, our observation that the NMC data are consistently low suggests that such a conclusion is incorrect.

We now investigate the consequence of our quark-nucleon Pomeron-exchange interaction in determining the energy dependence of vector meson electroproduction cross sections. The predicted energy dependence of ρ-meson and ϕ-meson photoproduction are shown as the upper and lower solid curves in Fig. 15, respectively. No parameters have been varied to obtain these results. Within our model, the rate of increase with energy is completely determined by the value of α_0. This is due to the assumption that the energy dependence of $G(s,t)$ in Eq. (2.5) can be calculated from the external legs, and hence the quark-loop integration in Eq. (4.20) only generates a t dependence. The results shown in Fig. 15 and previous figures indicate that this assumption is valid and sufficient to describe light-quark meson-hadron interactions. However, J/ψ-meson electroproduction has a much steeper W dependence which *cannot* be completely accounted for with $\alpha_0\approx 0.10$. This is discussed further in the next section.

At low energies, large-t contributions become important and other (nondiffractive) exchange mechanisms must be included to describe the ρ- and ϕ-meson electroproduction data. To demonstrate this, we have carried out a simple calculation using the lowest order meson-exchange contributions derived from the phenomenological Lagrangian of Ref.

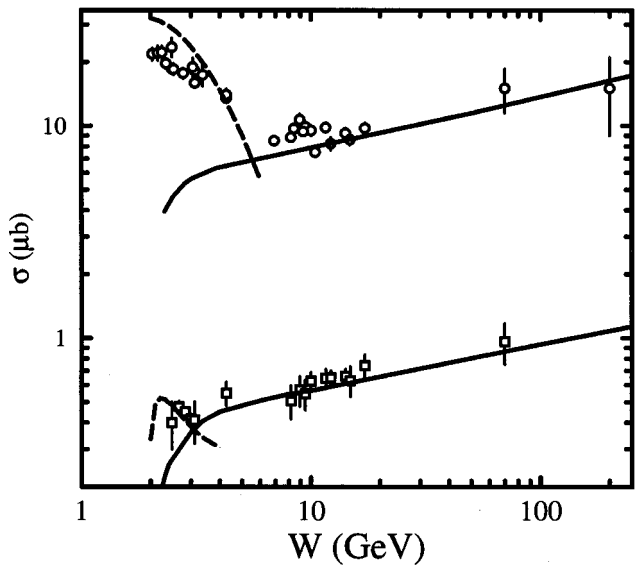

FIG. 15. Energy dependence of ρ- (top) and ϕ-meson (bottom) photoproduction cross sections. The solid curves are the predictions from our quark-nucleon Pomeron-exchange interaction. The dashed curves are the predictions of the meson-exchange model discussed in the text. The ρ-meson data (triangles) are from Refs. [35,36,44–47]. The ϕ-meson data (squares) are from Refs. [41,44,46,48].

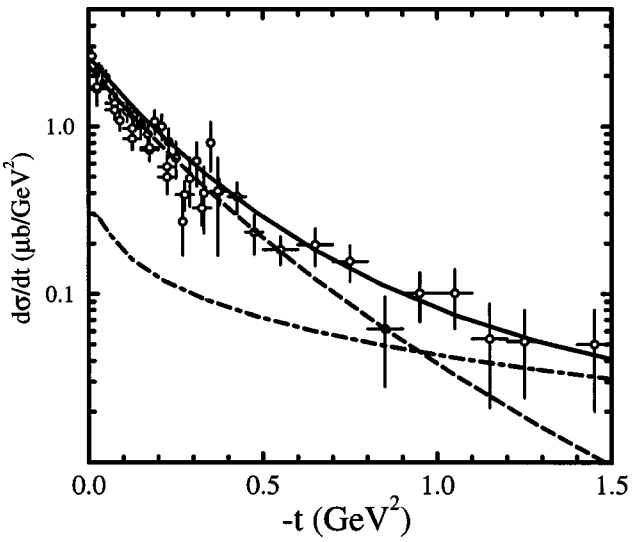

FIG. 16. The differential cross section for ϕ-meson photoproduction ($q^2=0$) for $3.0 \leqslant W \leqslant 3.5$ GeV. The dashed curve is the contribution due to the Pomeron-exchange interaction and the dot-dashed curve is the contribution due to π and η exchange at $W=3.0$ GeV. The solid curve is the sum of these. The data are from Refs. [48,51,52].

[49]. For ϕ-meson photoproduction, we only consider π and η exchanges and use the parameters from the Bonn potential [50] and experimental decay constants. We introduce a cutoff function $\Lambda^2/(\Lambda^2+k^2)$ with $\Lambda=1$ GeV, so that the magnitudes of the low-energy cross sections agree roughly with experiment. The resulting cross sections are shown as dashed curves in Fig. 15.

It is interesting to note that the meson-exchange contributions decrease with energy so that at sufficiently high energies Pomeron exchange dominates. We see from Fig. 15 that the W dependence of meson exchange is strikingly different than that of Pomeron exchange. This difference suggests that these two exchanges may be modeling very different aspects of QCD. For example, one might view meson exchange as a phenomenological representation of the exchange of correlated quark-antiquark pairs. Its strength, therefore, depends strongly on the flavor structure of the hadrons involved. Therefore, it is not then surprising that meson-exchange contributions to ϕ-meson photoproduction are significantly less than those to ρ-meson photoproduction; the lack of valence-s quarks in the nucleon tends to suppress direct quark exchanges. The fact that Pomeron exchange contributes similarly to both of these processes, independent of the flavor of the quark substructure of the hadrons involved (as shown in Fig. 15), is suggestive that the underlying mechanism of Pomeron exchange is multiple-gluon exchange. This idea was proposed long ago in Refs. [3,4] and is supported by much experimental evidence. Our results in Fig. 15 provide additional evidence in support of this notion. However, further theoretical work is necessary to make compelling the identification between Pomeron exchange and multiple-gluon exchange.

As a second illustration of the differences between Pomeron exchange and meson exchange in ϕ-meson photoproduction, we present our predictions for the differential cross section at $W=3$ GeV in Fig. 16. We observe that Pomeron exchange (dashed curve) is dominant in the forward peak while π and η exchanges (dot-dashed curve) contribute a flatter background. This is in accord with our expectation that Pomeron exchange is responsible for the diffractive, forward peak observed in these cross sections.

The absence of valence-s quarks in the nucleon tends to suppress meson-exchange contributions to ϕ-meson electroproduction. This provides the opportunity for experimental facilities, such as TJNAF, to probe the interplay between Pomeron exchange and meson exchange in processes such as ϕ-meson photoproduction. In particular, spin observables may be used to extract details concerning the Dirac structure of the quark-Pomeron-exchange coupling. Such studies could provide new insights into the QCD dynamics underlying Pomeron exchange.

C. Electroproduction of J/ψ mesons

The final process we consider is J/ψ-meson electroproduction. Although data is scarce and our treatment of the c-quark propagator is necessarily simplistic, it is nonetheless, instructive to perform an exploratory study of this process in our model.

It is observed that the J/ψ-meson photoproduction cross section rises more sharply with energy than do ρ- and ϕ-meson photoproduction cross sections. The energy dependence of our model is determined by the parameter α_0, and is, by construction, the same for all diffractive processes. Therefore, we anticipate the need to alter the value of α_0 to properly account for this energy dependence. We also find that the t dependence of J/ψ photoproduction predicted by our model is too steep. In this section, we allow a minimal flavor dependence of the model parameters necessary to provide a good description of J/ψ-meson electroproduction. Although the model does not predict the observed J/ψ photoproduction cross sections, we argue that our model of the

quark substructure of the J/ψ meson is sufficient and that it is our assumption of a flavor-dependent Pomeron-exchange amplitude that must be relaxed to obtain agreement with the data.

The c quark has not been studied to the extent that the u, d and s quarks have. Therefore, we develop a simple model c-quark propagator and consider the EM decay $J/\psi \to e^+e^-$ to determine the J/ψ-meson BS amplitude.

Numerical studies [30] suggest to us that the c-quark propagator can be more simply parametrized than the light-quark propagators. The heavy mass of the c quark, $m_c \approx 1.2$ GeV, provides the dominant scale in the propagator. This observation supports the use of a model c-quark propagator that exhibits confinement, reduces to the correct asymptotic form, required by perturbative QCD, but has only one momentum scale m_c. We, therefore, employ the model propagator

$$S_c(k) = (-i\gamma\cdot k + m_c)\frac{1-e^{-(1+k^2/m_c^2)}}{k^2+m_c^2}. \qquad (4.24)$$

There are fewer phenomenological constraints on the BS amplitude of the J/ψ meson since there is no J/ψ decay analogous to $\rho \to \pi\pi$; we have only $J/\psi \to e^+e^-$ to fix the parameters in the BS amplitude. To reduce the number of parameters in the vector-meson BS amplitude given in Eq. (4.1), we set $c_{J/\psi}=0$, thereby eliminating two of the parameters and the $1/k^2$ behavior of the amplitude. The BS amplitude is then

$$V_\mu(p,p') = \frac{1}{N_{J/\psi}} e^{-k^2/a_{J/\psi}^2}\left[\gamma_\mu + \frac{P_\mu \gamma\cdot P}{m_{J/\psi}^2}\right], \qquad (4.25)$$

where $P = p - p'$ is the total momentum of the J/ψ meson and $k = \frac{1}{2}(p+p')$ is the relative momentum between the quark and antiquark. The sole parameter $a_{J/\psi}$ is determined by reproducing the experimental decay width of $J/\psi \to e^+e^-$, using the procedure discussed in Sec. IV. The BS normalization $N_{J/\psi}$ is obtained from Eq. (4.2). The resulting value of $a_{J/\psi}$ and the calculated EM decay constant are given in Table III. The c-quark-Pomeron-exchange coupling constant β_c cannot be fixed from hadron-hadron elastic scattering since there are no data for the scattering of c-quark mesons from a nucleon target. Therefore, we choose the value of β_c such that the model reproduces the magnitude of the J/ψ-meson photoproduction ($q^2=0$) cross section at $W=100$ GeV from Ref. [53]. In contrast to ρ- and ϕ-meson electroproduction, the overall normalization of the J/ψ-meson electroproduction cross section is *not* a prediction of the model.

Upon substituting the BS amplitude of Eq. (4.25) and the c-quark propagator, Eq. (4.24), into Eq. (4.20) and multiplying by $\sqrt{8/9}$ (which arises from the flavor structure of the J/ψ meson), we obtain the photon-J/ψ-Pomeron-exchange transition amplitude $t_{\mu\alpha\nu}^{[J/\psi]}(q,P)$. This amplitude is then substituted into Eq. (4.19) to calculate the cross section for J/ψ-meson electroproduction.

The predicted q^2 dependence of the J/ψ-meson electroproduction cross section is the solid curve shown in Fig. 17 at $W=$ 100 GeV. Our prediction is in excellent agreement with the data. It is important to emphasize that *no* parameters were adjusted to obtain this result. As in the case of ρ- and ϕ-meson electroproduction, the q^2 dependence of the J/ψ electroproduction cross section arises solely from the quark-loop integration and hence is a *prediction* of our model.

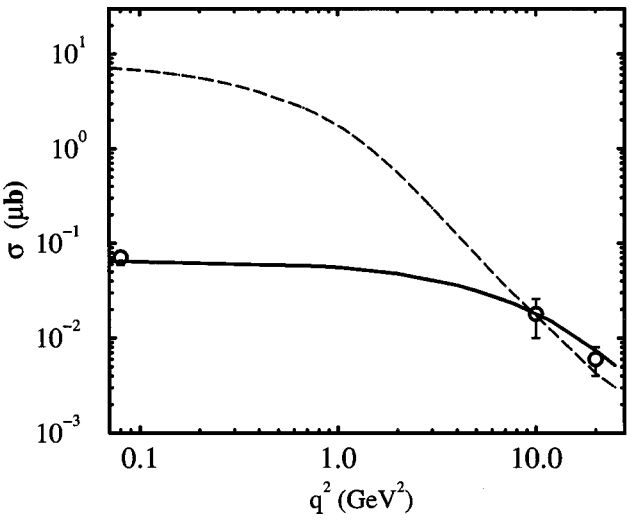

FIG. 17. The total J/ψ-meson electroproduction cross section at $W=$ 100 GeV (solid curve) and total ρ-meson electroproduction cross section at $W=15$ GeV (dashed curve). The J/ψ-meson data are from Refs. [53,54].

In the same figure, for comparison, we also display our results for ρ-meson electroproduction. The presence of heavy c quarks dramatically changes the q^2 dependence of the cross section. (This was anticipated from our analysis of the q^2 dependence of ρ and ϕ-meson electroproduction in Secs. IV A and IV B.) Remarkably, although the J/ψ-meson photoproduction ($q^2=0$) cross section is two orders of magnitude lower than that for the ρ meson, they are equal at $q^2 \approx 15$ GeV^2. (We note that the curves shown in Fig. 17 are evaluated at *different* energies. When the energy dependence of the ρ-meson cross section is taken into account, the two curves intersect at $q^2 \approx 15$ GeV^2.) This surprising result arises naturally in our model as a consequence of the dynamical treatment of the quark loop which was shown, in Sec. IV A, to depend on the current-quark mass m_f. Future experimental data for J/ψ-meson electroproduction, especially at moderate q^2, would be helpful to confirm our predictions.

In Fig. 18, our prediction of the differential cross section for J/ψ-meson photoproduction is compared to the data of Ref. [53]. The resulting solid curve fails to reproduce the observed t dependence of the data. In our model, there are three sources of t dependence: the nucleon form factor $F_1(t)$ in Eq. (2.6), the Pomeron-exchange amplitude $G(s,t)$ in Eq. (2.5), and the photon-J/ψ-Pomeron-exchange coupling $t_{\mu\alpha\nu}^{[J/\psi]}(q,P)$.

In this exclusive process, the requirement that a J/ψ meson is produced and the nucleon does *not* break up, introduces a t dependence. This t dependence should be present in any model. We can estimate the effect of these two constraints on the t dependence by setting $\alpha_1=0$ in Eq. (2.5). The resulting cross section is shown as a dashed curve in Fig. 18. This curve can be represented as the net t depen-

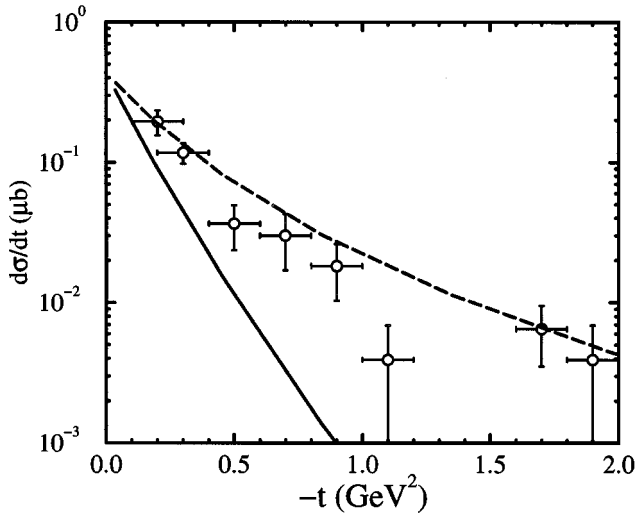

FIG. 18. The differential cross section for J/ψ-meson photoproduction ($q^2=0$). The solid curve is our result at $W=$ 40 GeV. The dashed curve is an estimation of the contribution to the differential cross section from the quark substructure of the J/ψ meson and nucleon. The data are from Ref. [53].

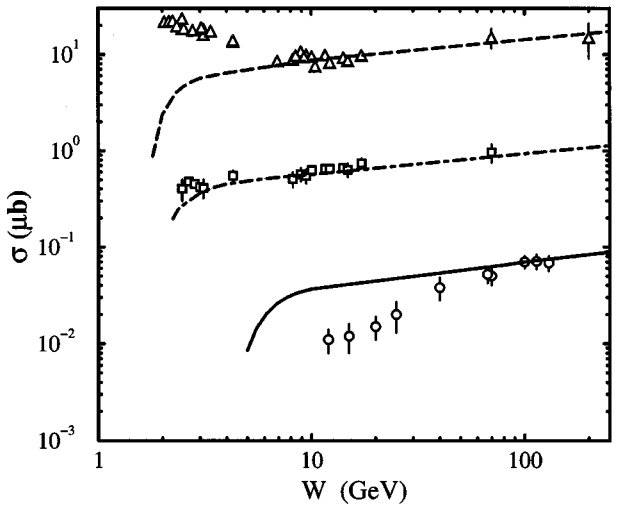

FIG. 19. The predicted energy evolution of vector-meson photoproduction ($q^2=0$) for ρ (dashed curve), ϕ (dot-dashed curve), and J/ψ mesons (solid curve). The data are from Refs. [44,53,54].

dence arising from the quark substructure of the J/ψ meson [$t^{[J/\psi]}_{\mu\alpha\nu}(q,P)$ from Eq. (4.20)] and the nucleon [$\approx F_1(t)$ in Eq. (2.6)]. As such, it represents a bound on the t dependence of the cross section. The data in Fig. 18 are consistent with this interpretation in that they lie below the predicted bound.

Furthermore, in Sec. IV A, we have shown that the q^2 dependence of vector-meson electroproduction arises entirely from the quark substructure of the vector meson. The fact that our model readily reproduces the observed q^2 dependence J/ψ electroproduction (see Fig. 17) suggests that the amplitude $t^{[J/\psi]}_{\mu\alpha\nu}(q,P)$ provides an adequate description of the quark substructure of the J/ψ meson. Therefore, we believe that the discrepancy between our result (solid curve) and the data in Fig. 18 is due to having employed the value $\alpha_1=$ 0.33 GeV^{-2} obtained from our study of πN elastic scattering. We suspect that the assumed flavor independence of the parameters α_0 and α_1 is sufficient to describe diffractive processes involving light quarks, but that it is too restrictive to provide agreement with the data for J/ψ-meson electroproduction. By relaxing this constraint, the data in Fig. 18, for $t\leqslant -1.3$ GeV^2, are reproduced with $\alpha_1^c=0.10$ GeV^{-2}.

As indicated earlier, the energy dependence of J/ψ photoproduction is much stronger than the other processes we have considered. Our results for J/ψ-meson photoproduction are plotted versus W in Fig. 19 along with our results for the ρ and ϕ mesons. The W dependence obtained from our model for J/ψ photoproduction is not in agreement with the data. However, by relaxing the flavor-independence assumption in the model, one can account for this steep energy dependence. The data for J/ψ-meson photoproduction shown in Fig. 19 (circles) are reproduced by choosing $\alpha_0^c=0.42$.

It has been suggested [26] that the discrepancy between the W and t dependence of J/ψ electroproduction and that of ρ- or ϕ-meson electroproduction could be explained if the energies at which current experiments are conducted are not yet in the asymptotic region that would be well described by Pomeron exchange. Further experimental data on the diffractive electroproduction of the J/ψ meson at higher energies would help to test this hypothesis.

This concludes our discussion of J/ψ-meson electroproduction. We find that we can obtain good agreement with all data provided only that we relax our model assumption that the Pomeron-exchange parameters be independent of the flavor of the quarks involved.

V. SUMMARY AND CONCLUSIONS

In this paper, we have developed a model quark-nucleon Pomeron-exchange interaction and employed it in a study of the role of the quark substructure of mesons in meson-nucleon elastic scattering and exclusive vector-meson electroproduction on nucleons. The quark substructure of the mesons is described in terms of relativistic quark-antiquark Bethe-Salpeter amplitudes within a framework developed from phenomenological studies of the Dyson-Schwinger equations of QCD. The model developed herein provides a framework in which some of the crucial aspects of nonperturbative-quark dynamics can be explored in diffractive processes. As such, this work represents a first attempt to separate the effects of hadron substructure from the effects of Pomeron exchange on the observables of diffractive processes. This separation is a necessary step toward the development of an understanding of the quark and gluon dynamics underlying Pomeron exchange.

The quark-nucleon Pomeron-exchange interaction, introduced in Sec. II, is defined in terms of four parameters. They are determined by requiring that the model reproduce πN and KN elastic scattering data. The model interaction is then used to predict the electroproduction of ρ and ϕ mesons on nucleons. We find that the model successfully describes both the slopes and magnitudes of the differential cross sections. The predicted energy and q^2 dependence of the ρ- and ϕ-meson photoproduction cross sections are in excellent agreement with the data.

For these process, Pomeron exchange provides the domi-

nant contribution for large energies, but as the energy is decreased, other mechanisms come into play. Meson exchanges contribute significantly at energies $W \leqslant 6$ GeV for ρ-meson electroproduction and $W \leqslant 3$ GeV for ϕ-meson electroproduction. If meson exchange can be identified with correlated quark-antiquark exchange then the dramatically different behaviors predicted from the meson- and Pomeron-exchange mechanisms support the notion that the dynamics underlying Pomeron exchange would be best described in terms of gluon degrees of freedom. Future work will address this intriguing possibility.

The observed asymptotic $1/q^4$ dependence of vector-meson electroproduction cross sections arises naturally from the quark substructure of the vector meson. Our predictions are different from those of other authors and are in agreement with the recent data from HERA for ρ-, ϕ-, and J/ψ-meson diffractive electroproduction. We show that the scale that determines the onset of this asymptotic behavior is determined by the current-quark mass of the quarks inside the vector meson. This work elucidates the relationship between the q^2 dependence of diffractive electroproduction cross sections and the current-quark mass. This important observation explains the dramatic differences between the q^2 dependence seen in the electroproduction cross sections of the various vector mesons.

We also find that the normalization of both ρ- and ϕ-meson electroproduction data from NMC are too low to be accounted for by our model. This is based on our analysis, in Sec. IV, of the role played by the current-quark mass in determining the onset of the asymptotic $1/q^4$ behavior in vector-meson electroproduction. This finding is particularly important because these data have been used to suggest that large-q^2 electroproduction cross sections have a stronger energy dependence than that which is observed in low-q^2 electroproduction and elastic hadron-hadron scattering. However, our results suggest that these NMC data do not represent an accurate measure of vector meson electroproduction on a *nucleon*, hence such a conclusion cannot be drawn.

In an exploratory investigation of J/ψ-meson electroproduction, we find that although the q^2 dependence of the cross section is correctly predicted by our model, the observed energy dependence is much steeper and the t dependence much flatter than those we obtain. This discrepancy between our model and the experimental data can be removed by allowing a flavor dependence in the quark-nucleon Pomeron-exchange interaction.

In this work, we have given an indication of the important role played by the quark substructure of hadrons in exclusive, diffractive processes. In particular, the q^2 dependence of electroproduction cross sections is a sensitive probe of the dynamical evolution of the confined quark from the domain in which nonperturbative dressing effects are important to that in which it behaves as a current quark. We also find that the minimal dressing of the quark-photon vertex, required by the Ward-Takahashi identity, keeps the exclusive vector-meson electroproduction cross section from reaching a naive perturbative-QCD limit as q^2 becomes large. Hence, there are *always* some nonperturbative contributions to these exclusive processes. One observable that is particularly sensitive to the nonperturbative dressing of the quark-photon vertex is the ratio of longitudinal to transverse electroproduction cross sections R. Future experimental measurements of R will provide an important tool with which to investigate the importance of the nonperturbative dressing of the quark-photon vertex.

In conclusion, we have developed a model quark-nucleon Pomeron-exchange interaction that successfully describes the extensive data for diffractive processes on the nucleon. A framework developed from studies of the Dyson-Schwinger equations of QCD was employed to describe the quark substructure of mesons. Our results indicate that such a framework can provide a uniformly good description of exclusive processes at both low and high energies. We argue that the quark substructure of vector mesons plays a central role in determining the behavior of the electroproduction cross sections considered, particularly the q^2 dependence of the cross section. Our results are consistent with the notion that Pomeron exchange may be identified with a multiple-gluon exchange mechanism within QCD. However, further work is required to make this possible identification compelling. Such an investigation requires a careful treatment of the quark substructure of hadrons.

ACKNOWLEDGMENTS

The authors are grateful to C.D. Roberts for many stimulating conversations and helpful suggestions. This work was supported by the U.S. Department of Energy, Nuclear Physics Division, under Contract No. W-31-109-ENG-38. M.A.P. also received support from the Division of Educational Programs at Argonne National Laboratory and the Dean of Graduate Studies of the Faculty of Arts and Sciences of the University of Pittsburgh. The computations described herein were carried out using resources at the National Energy Research Scientific Computing Center.

[1] J. B. D. Collins, *An Introduction to Regge Theory and High Energy Physics* (Cambridge University Press, Cambridge, England, 1977).

[2] A. C. Irving and R. P. Worden, Phys. Rep. **34**, 117 (1977).

[3] F. E. Low, Phys. Rev. D **12**, 163 (1975).

[4] S. Nussinov, Phys. Rev. D **34**, 1286 (1975).

[5] A. Donnacie and P. V. Landshoff, Nucl. Phys. **B244**, 322 (1984).

[6] A. Donnachie and P. V. Landshoff, Phys. Lett. B **185**, 403 (1987).

[7] J.-M. Laget and R. Mendez-Galain, Nucl. Phys. **A581**, 397 (1995).

[8] M. A. Pichowsky and T.-S. H. Lee, Phys. Lett. B **379**, 1 (1996).

[9] M. R. Pennington, *Calculating Hadronic Properties in Strong QCD*, talk given at 2nd Workshop on ELFE Physics, 1996,

Report No. hep-ph/9611242, 1996 (unpublished).
[10] C. D. Roberts and A. G. Williams, Prog. Part. Nucl. Phys. **33**, 477 (1994).
[11] M. R. Frank and C. D. Roberts, Phys. Rev. C **53**, 390 (1996).
[12] C. J. Burden, C. D. Roberts, and M. J. Thomson, Phys. Lett. B **371**, 163 (1996).
[13] C. D. Roberts, Nucl. Phys. **A605**, 475 (1996).
[14] P. C. Tandy, Prog. Part. Nucl. Phys. **36**, 97 (1996).
[15] R. Alkofer and C. D. Roberts, Phys. Lett. B **369**, 101 (1996).
[16] M. R. Frank, K. L. Mitchell, C. D. Roberts, and P. C. Tandy, Phys. Lett. B **359**, 17 (1995).
[17] Yu. Kalinovsky, K. L. Mitchell, and C. D. Roberts, Report No. nucl-th/9610047, ANL-PHY-8585-TH-96, 1996 (unpublished).
[18] S. J. Brodsky, L. Frankfurt, J. F. Gunion, A. H. Mueller, and M. Strikman, Phys. Rev. D **50**, 3134 (1994).
[19] M. G. Ryskin, R. G. Roberts, A. D. Martin, and E. M. Levin, Report No. hep-ph/9511228 v2, 1996 (unpublished).
[20] I. F. Ginzburg and D. Yu. Ivanov, Phys. Rev. D **54**, 5523 (1996).
[21] H. G. Dosch, T. Gousset, G. Kulzinger, and H. J. Pirner, Phys. Rev. D **55**, 2602 (1997).
[22] A. D. Martin, M. G. Ryskin, and T. Teubner, Phys. Rev. D **55**, 4329 (1997).
[23] L. Frankfurt, W. Koepf, and M. Stikman, Phys. Rev. D **54**, 3194 (1996).
[24] J. C. Collins, L. Frankfurt, and M. Strikman, Report No. hep-ph/9611433, 1996 (unpublished).
[25] J. R. Cudell and I. Royen, Report No. hep-ph/9609490, 1996 (unpublished).
[26] L. L. Jenkovszky, E. S. Martynov, and F. Paccanoni, Report No. hep-ph/9608384, 1996 (unpublished).
[27] J. R. Cudell, K. Kang, and S. K. Kim, Report No. hep-ph/9601336, 1996 (unpublished).
[28] A. Bender, C. D. Roberts, and L. v. Smekal, Phys. Lett. B **380**, 7 (1996).
[29] C. W. Akerlof *et al.*, Phys. Rev. D **14**, 2864 (1976).
[30] P. Jain and H. J. Munczek, Phys. Rev. D **46**, 438 (1992); **48**, 5403 (1993).
[31] Particle Data Group, L. Montanet *et al.*, Phys. Rev. D **50**, 1173 (1994), pp. 1457–1458.
[32] A. Bashir and M. R. Pennington, Phys. Rev. D **50**, 7679 (1994).
[33] J. S. Ball and T.-W. Chiu, Phys. Rev. D **22**, 2542 (1980).
[34] C. W. Akerlof, W. W. Ash, K. Berkelman, and C. A. Lichtenstein, Phys. Rev. **163**, 1482 (1967); L. N. Hand, *ibid.* **129**, 1834 (1963); K. Schilling and G. Wolf, Nucl. Phys. **B61**, 381 (1973).
[35] ZEUS Collaboration, M. Derrick *et al.*, Z. Phys. C **69**, 39 (1995).
[36] W. D. Shambroom *et al.*, Phys. Rev. D **26**, 1 (1982).
[37] J. J. Aubert *et al.*, Phys. Lett. **161B**, 203 (1985).
[38] M. Arneodo *et al.*, Nucl. Phys. **B429**, 503 (1994).
[39] ZEUS Collaboration, M. Derrick *et al.*, Phys. Lett. B **356**, 601 (1995).
[40] ZEUS Collaboration, M. Derrick *et al.*, *High Q^2 Exclusive Vector Meson Production at HERA*, Proceedings of the XXVIII International Conference on High Energy Physics, Warsaw, 1996 (unpublished).
[41] ZEUS Collaboration, M. Derrick *et al.*, Phys. Lett. B **377**, 259 (1996).
[42] ZEUS Collaboration, M. Derrick *et al.*, Phys. Lett. B **380**, 220 (1996).
[43] D. Geesaman (private communication); E665 Collaboration, M. R. Adams *et al.*, MPI Report No. MPI-PhE/97-03 (unpublished).
[44] J. Ballam *et al.*, Phys. Rev. D **7**, 3150 (1973).
[45] W. Struczinski *et al.*, Nucl. Phys. **B108**, 45 (1976).
[46] R. M. Egloff *et al.*, Phys. Rev. Lett. **43**, 657 (1979).
[47] D. Aston *et al.*, Nucl. Phys. **B209**, 56 (1982).
[48] D. P. Barber *et al.*, Z. Phys. C **12**, 1 (1983).
[49] T. Sato and T.-S. H. Lee, Phys. Rev. C **54**, 2660 (1996).
[50] R. Macheleidt, in *Advances in Nuclear Physics*, edited by J.W. Negele and E. Vogt (Plenum, New York, 1989), Vol. 19.
[51] D. P. Barber *et al.*, Phys. Lett. **79B**, 150 (1978).
[52] H. J. Behrend *et al.*, Nucl. Phys. **B144**, 22 (1978).
[53] ZEUS Collaboration, M. Derrick *et al.*, Phys. Lett. B **350**, 120 (1995).
[54] H1 Collaboration, S. Aid *et al.*, Nucl. Phys. **B468**, 3 (1996).